

## ROBOTIC LASER-ADAPTIVE-OPTICS IMAGING OF 715 KEPLER EXOPLANET CANDIDATES USING ROBO-AO

NICHOLAS M. LAW<sup>1</sup>, TIM MORTON<sup>2</sup>, CHRISTOPH BARANEC<sup>3</sup>, REED RIDDLE<sup>2</sup>, GANESH RAVICHANDRAN<sup>4</sup>, CARL ZIEGLER<sup>1</sup>, JOHN ASHER JOHNSON<sup>5</sup>, SHRIHARSH P. TENDULKAR<sup>2</sup>, KHANH BUI<sup>2</sup>, MAHESH P. BURSE<sup>6</sup>, H. K. DAS<sup>6</sup>, RICHARD G. DEKANY<sup>2</sup>, SHRINIVAS KULKARNI<sup>2</sup>, SUJIT PUNNADI<sup>2</sup>, A. N. RAMAPRAKASH<sup>6</sup>

*Draft version November 15, 2021*

### ABSTRACT

The Robo-AO *Kepler* Planetary Candidate Survey is designed to observe every *Kepler* planet candidate host star with laser adaptive optics imaging to search for blended nearby stars, which may be physically associated companions and/or responsible for transit false positives. In this paper we present the results from the 2012 observing season, searching for stars close to 715 representative *Kepler* planet candidate hosts. We find 53 companions, 44 of which are new discoveries. We detail the Robo-AO survey data reduction methods including a method of using the large ensemble of target observations as mutual point-spread-function references, along with a new automated companion-detection algorithm designed for large adaptive optics surveys. Our survey is sensitive to objects from  $\approx 0''.15$  to  $2''.5$  separation, with contrast ratios up to  $\Delta m \approx 6$ . We measure an overall nearby-star-probability for *Kepler* planet candidates of  $7.4\% \pm 1.0\%$ , and calculate the effects of each detected nearby star on the *Kepler*-measured planetary radius. We discuss several KOIs of particular interest, including KOI-191 and KOI-1151, which are both multi-planet systems with detected stellar companions whose unusual planetary system architecture might be best explained if they are "coincident multiple" systems, with several transiting planets shared between the two stars. Finally, we detect  $2.6\sigma$  evidence for  $< 15d$ -period giant planets being  $2-3\times$  more likely to be found in wide stellar binaries than smaller close-in planets and all sizes of further-out planets.

### 1. INTRODUCTION

The *Kepler* mission, which has searched approximately 190,000 stars for the tiny periodic dips in stellar brightness indicative of transiting planets, is unprecedented in both sensitivity and scale among transiting planet surveys (Koch et al. 2010). Never before has a survey been able to detect such small planets—down to even the size of the Earth’s moon (Barclay et al. 2013)—and never before has a survey delivered so many planet candidates, with over 3500 planet candidates (candidate *Kepler* Objects of Interest; KOIs) found in a search of the first twelve quarters of *Kepler* photometry (Borucki et al. 2010, 2011; Batalha et al. 2013a,b; Tenenbaum et al. 2013).

All transit surveys require follow-up observations of the detected candidates. The purpose of this follow-up is twofold: first to confirm that the detected photometric dimmings are in fact truly transiting planets rather than astrophysical false positives; and second to characterize the host stellar system. High-angular-resolution imaging is a crucial ingredient of the follow-up effort, as many astrophysical false positive scenarios involve nearby stellar systems whose light is blended with the target star (e.g.

O’Donovan et al. 2006). Even if a transit candidate is a true planet, identifying whether it is in a binary stellar system has potentially important implications for determining the planet’s detailed properties. For example, if there is considerable diluting flux from a companion star within the photometric aperture, even if the planet interpretation of the signal is secure, the planet will be larger than implied by the light curve alone under the assumption of a single host star (e.g. Johnson et al. 2011). The presence or absence of third bodies in the systems can also have broader implications about the processes of planetary system formation and evolution; stellar binarity has been hypothesized to be important in shaping the architectures of planetary systems, both by regulating planet formation and by dynamically sculpting planets final orbits, such as forcing Kozai oscillations that cause planet migration (e.g. Fabrycky & Tremaine 2007; Katz et al. 2011; Naoz et al. 2012) or tilting the circumstellar disk (Batygin 2012).

The vast majority of the individual *Kepler* candidates remain unconfirmed (<3% currently confirmed according to the NASA Exoplanet Archive [NEA]). Current predictions based on models of the expected population of confusion sources suggest that at least 10-15% of *Kepler*’s planetary candidates may be astrophysical false positives and that a large fraction of confirmed planets also have incorrectly determined planetary parameters because of confusing sources (Morton & Johnson 2011; Fressin et al. 2013; Dressing & Charbonneau 2013; Santerne et al. 2013). The possible false-positive scenario probabilities change with the brightness of the *Kepler* target, the details of its *Kepler* light curve, its spectral type, and the properties of the detected planetary system (e.g. Morton 2012). The false positives thus limit

<sup>1</sup> Department of Physics and Astronomy, University of North Carolina at Chapel Hill, Chapel Hill, NC 27599-3255, USA

<sup>2</sup> Division of Physics, Mathematics, and Astronomy, California Institute of Technology, Pasadena, CA, 91125, USA

<sup>3</sup> Institute for Astronomy, University of Hawai’i at Mānoa, Hilo, HI 96720-2700, USA

<sup>4</sup> W. Tesper Clarke High School, East Meadow School District, 740 Edgewood Dr Westbury, NY 11590, USA

<sup>5</sup> Harvard-Smithsonian Center for Astrophysics, 60 Garden St., Cambridge, MA 02138

<sup>6</sup> Inter-University Centre for Astronomy & Astrophysics, Ganeshkhind, Pune, 411007, India

our ability to interpret individual objects, to evaluate differences in planetary statistics between different stellar populations, and to generate fully robust statistical studies of the planetary population seen by *Kepler*.

In order to fully validate the individual *Kepler* planets and search for correlations between planetary systems and stellar multiplicity properties, we need to measure the companion population around every *Kepler* Object of Interest. There have been several high-angular-resolution surveys of selected samples of KOIs to detect stellar companions and assess the false-positive probability (Adams et al. 2012; Lillo-Box et al. 2012; Horch et al. 2012; Barrado et al. 2013). However, the overheads typically associated with ground-based adaptive optics imaging have limited the number of targets which can be observed.

In this paper we present the first results from a laser-adaptive-optics survey that takes short snapshot high-angular-resolution images of every *Kepler* planet candidate. The survey uses Robo-AO, the first robotic laser adaptive optics system (Baranec et al. 2012, 2013). We designed the automated system for relatively high time-efficiency, with an overhead of 90-seconds including target-to-target slew time. This speed allows Robo-AO to take high-angular-resolution snapshot images of 20-25 targets per hour, allowing the *Kepler* target list to be completed in less than 150 hours of observing time. This paper presents the 2012-observing-season results of the ongoing Robo-AO KOI survey, covering 715 targets and finding 53 companions<sup>7</sup>, 44 of them new discoveries.

The paper is organized as follows: in §2 we describe the Robo-AO system and the KOI survey target selection and observations. §3 describes the Robo-AO data reduction and companion-detection pipeline. In §4 we describe the survey’s results, including the discovered companions. We discuss the results in §5, including detailing the effects of the survey’s discoveries on the interpretation and veracity of the observed KOIs, and a brief discussion of the *Kepler* planet candidates’ overall binarity statistics. We conclude in §6.

## 2. OBSERVATIONS & DATA REDUCTION

We used Robo-AO to obtain 90-second-exposure high-angular-resolution images of 715 *Kepler* planet candidate host stars in summer 2012. We performed all the observations in a queue-scheduled mode with the Robo-AO laser adaptive optics system (Baranec et al. 2012) mounted on the robotic Palomar 60-inch telescope (Cenko et al. 2006). The survey and system specifications are summarized in table 1.

### 2.1. The Robo-AO Laser Adaptive Optics System

Robo-AO is a laser-guide-star adaptive optics system engineered for high-efficiency autonomous observing on 1- to 3-m-class telescopes (Baranec et al. 2013, 2012; Riddle et al. 2012). With few-minute exposures and target-to-target overheads of  $\leq 90$ s, Robo-AO typically observes 200-250 targets per night. The system uses a UV Rayleigh-scattering laser to generate a bright artificial guide star near all its targets and typically delivers

<sup>7</sup> for brevity we denote stars which we found within our detection radius of KOIs as “companions”, in the sense that they are asterisms associated on the sky. In §5 we evaluate the probability that the detected objects are actually physically associated.

TABLE 1  
THE SPECIFICATIONS OF THE ROBO-AO KOI SURVEY

#### Robo-AO specifications

Telescope	Palomar 60-inch telescope
Science camera	Andor iXon DU-888
EMCCD detector	E2V CCD201-20
EM gain setting	100-300
Effective read-noise	0.16-0.48 e <sup>-</sup>
Full-frame-transfer readout	8.6 frames/sec
Detector format	1024 <sup>2</sup> pixels
Pixel scale	43.1 mas / pix
Field of view	44'' × 44''

#### KOI survey specifications

KOI targets observed	715
Exposure time	90 seconds
Observation wavelengths	600-950nm
Typical FWHM resolution	0''.12 – 0''.15
Typical contrast ratio at 0.5''	$\Delta = 5$ mags.
Observation date range	June 17 2012 – October 6 2012
Total observing time	36 hours
Targets observed / hour	20
LGS-AO overheads / target	≤90 seconds (inc. slew)

images with diffraction-limited 0''.12 – 0''.15 FWHM and Strehls of 10–25% at visible wavelengths. The science camera used for this imaging survey uses an electron-multiplying CCD (EMCCD) detector to achieve sub-electron read-noise at a full frame rate readout of 8.6 frames per second. The 1024<sup>2</sup> array is sampled at 43.1 mas pix<sup>-1</sup>, Nyquist sampled on the 60-inch telescope at wavelengths longer than 630nm.

The laser adaptive optics system corrects high-order wavefront aberrations with a closed-loop control rate of 1.2KHz, significantly sharpening the instantaneous point spread function (PSF) across the science camera’s field of view. However, a sufficiently bright star within that field is still required to correct residual stellar image motion in post-facto processing. Under typical observing conditions with a broad-band science filter selected, the system requires a target star brighter than  $M \approx 16.0$ , with narrower filters requiring brighter stars.

For the observations described here we used either a Sloan i'-band filter (York et al. 2000) or a long-pass filter cutting on at 600nm (LP600 hereafter). The latter filter roughly matches the *Kepler* passband (Figure 1) at the redder wavelengths while suppressing the blue wavelengths which have reduced adaptive optics performance (except in the very best seeing conditions). Compared to near-infrared adaptive optics observations, this filter more closely approximates direct measurement of the effects of unresolved companions on the *Kepler* light curves.

### 2.2. Target selection

We selected targets from the *Kepler* Objects of Interest (KOIs) catalog based on a Q1-Q6 *Kepler* data search (Batalha et al. 2013a). Our initial targets were selected randomly from the Q1-Q6 KOIs, requiring only that the targets are brighter than  $m_i = 16.0$ , a restriction which removed only 2% of the KOIs. While it is our intent to observe every KOI with Robo-AO, this initial target selection provides a representative coverage of the range of KOI properties. Given the Robo-AO’s low time overheads, we took the time to re-observe KOIs which already had detected companions, to produce a complete

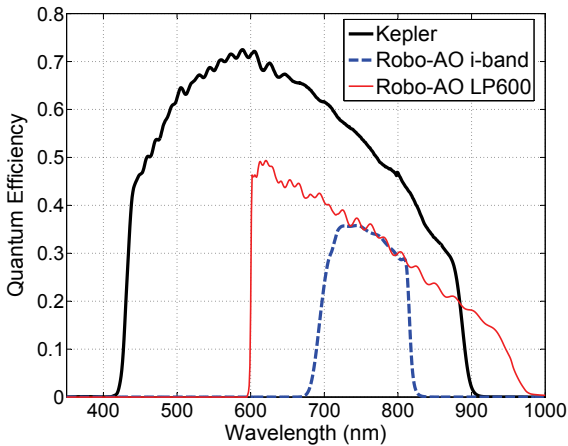


FIG. 1.— The *Kepler* and Robo-AO passbands. The Robo-AO curves are generated from measured reflection and transmission data from all optical components with the exception of the primary and secondary of the 60-inch telescope which are assumed to be ideal bare aluminum. The *Kepler* curve is adapted from the *Kepler* Instrument Handbook.

and homogenous survey.

In Figure 2 we compare the Robo-AO imaged KOIs to the distribution of all Batalha et al. (2013a) KOIs in magnitude, planetary period, planetary radius and stellar temperature. The Robo-AO list closely follows the KOI list in the range of magnitude covered, with the exception of the three brightest stars (which have already been covered in detail by other non-laser adaptive optics systems), and a reduced coverage of the faintest KOIs, which Robo-AO requires excellent weather conditions to reach. In planetary radius and period Robo-AO’s target distribution closely matches the full KOI list. Finally, in temperature, the target distribution again matches the KOI distribution with the exception of the few coolest (most faint) and hottest (most bright) KOIs. The false-positive and stellar multiplicity statistics we derive from the survey are thus likely to closely match the properties of the full ensemble of *Kepler* targets.

### 2.3. Observations

We used Robo-AO to observe 715 *Kepler* planet host stars between June 17 2012 and October 6 2012, on 23 separate nights (detailed in the table in the appendix). We observed in the LP600 and Sloan i'-band filters, acquiring 90-second total exposures of each target. We chose the 90-second exposure time to provide a snapshot image which would contain all sources likely to affect the *Kepler* light curve, including close-in sources up to  $\sim 5$  magnitudes fainter than the *Kepler* target. As far as possible, observing setting were kept constant between the KOIs to produce a homogenous survey. Each exposure consisted of 775 frames taken at 8.6 frames/sec, with an inter-frame dead time (during frame transfer) of 1.7 ms. Each series of frames was processed into single images which were then searched for companions (Section 3).

Two dominant factors affect Robo-AO’s imaging performance: the seeing and the brightness of the target. During the 23 nights of observing the median seeing was  $1.^{\prime\prime}2$ , with minimum and maximum values of  $0.^{\prime\prime}8$  and  $1.^{\prime\prime}9$  respectively. We developed an automated routine to

measure the actual imaging performance and to classify the targets into the imaging-performance classes given in the full observations list; these classes can be used with the contrast curve for each class to estimate the companion-detection performance for each target (§3.3).

## 3. DATA REDUCTION

To search the large dataset for companions we developed a fully-automated pipeline for data reduction, PSF subtraction, companion detection and companion measurements in Robo-AO data. The pipeline first takes the short-exposure data cubes recorded by the EMCCD camera and produces dark, flat-field and tip-tilt-corrected co-added output images (§3.1). We then subtract a locally-optimized point-spread-function (PSF) estimate from the image of the *Kepler* target in each field (§3.2), and then either detect companions around the target stars (§3.3) or place limits on their existence. Finally, we measured the properties of the detected companions (§3.4).

### 3.1. Imaging pipeline

The imaging pipeline is based on the Lucky Imaging reduction system described in Law et al. (2006a, 2009, 2012); Terziev et al. (2013). We briefly summarize the method here.

Each input frame is first dark-subtracted and flat-fielded using daytime calibrations. The frames are next corrected for image motion. In a pre-processing step the pipeline automatically selects a bright guide star near the center of the Robo-AO exposure. The region around the star is up-sampled by a factor of four using a cubic interpolation, and the resulting image is cross-correlated with a diffraction-limited point spread function for that wavelength (this has been shown to obtain much higher quality results than centroid or brightest-pixel alignment (e.g. Law et al. 2006a)). The frame is then shifted to align the position of greatest correlation to that of the other frames in the observation, and the stack of frames is co-added using the Drizzle algorithm (Fruchter & Hook 2002) to produce a final high-resolution output image sampled at twice the resolution of the input images.

For the KOI observations the relatively crowded fields often led to the automatic selection of a different guide star from the KOI. To avoid having to account for the effects of tip/tilt anisoplanatism, we manually checked the location of the KOI in Digital Sky Survey images and selected the KOI itself as the guide star in each observation. To produce more consistent and predictable imaging performance for groups of similar KOIs, we used the KOI even if a brighter guide was nearby and offered potentially increased performance.

### 3.2. PSF subtraction using the large set of Robo-AO target observations

The KOI target stars are all in similar parts of the sky, have similar brightness, and were observed at similar airmasses. Because it is extremely unlikely that a companion would be found in the same position for two different targets, we can use each night’s ensemble of (at least 20) KOI observations as PSF references without requiring separate observations.

We use a custom locally-optimized PSF subtraction routine based on the LOCI algorithm (Locally Optimized

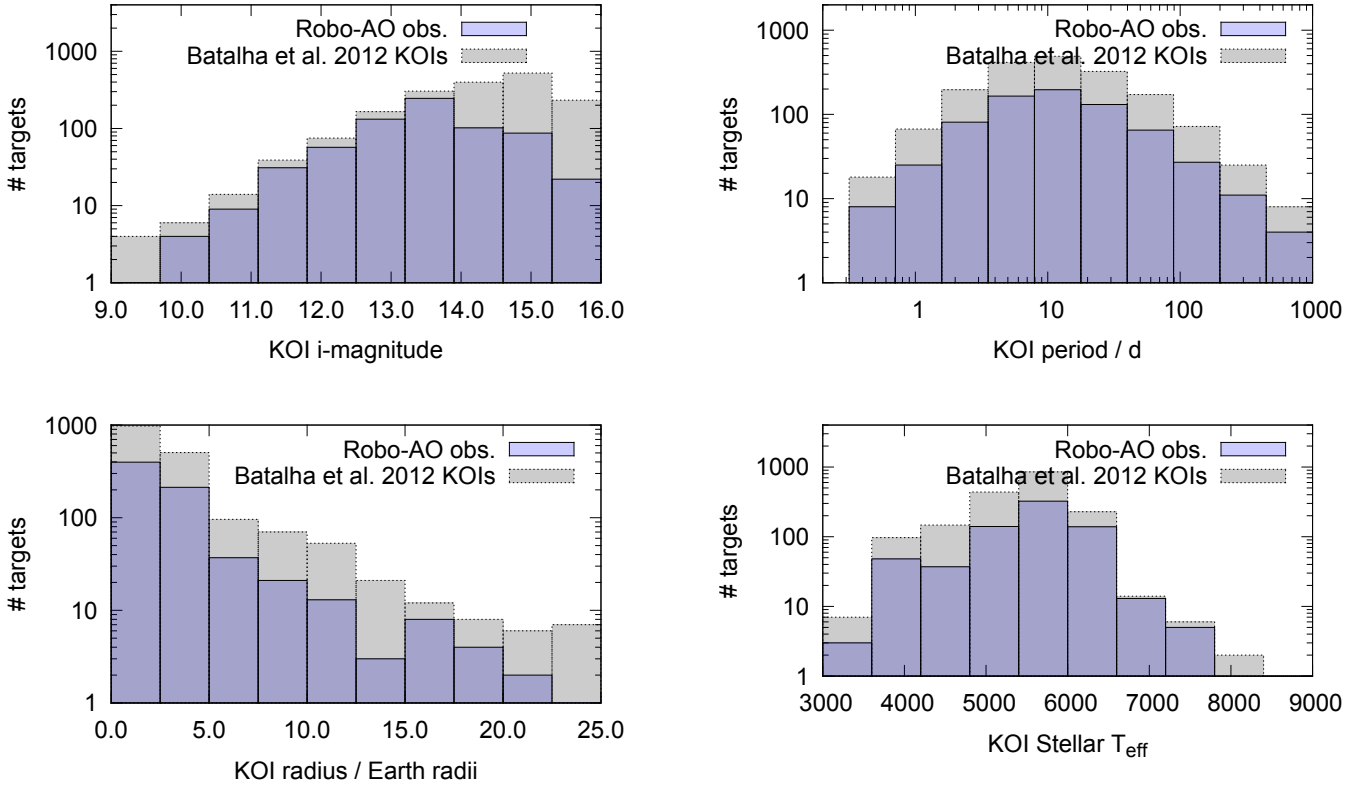


FIG. 2.— The distribution of the Robo-AO sample compared to the Batalha et al. (2013a) KOIs.

Combination of Images; (Lafrenière et al. 2007)). For each KOI target we select 20 other KOI observations obtained in the same filter and closest to the target observation in time. We then divide the region around the target star into sections based on polar coordinates: 5 upsampled pixels (110 mas) in radius and 45 degrees in angle. Similar sections are extracted from each PSF reference image.

We then generate a locally-optimized estimate of the PSF in each section by generating linear combinations of the reference PSFs. In each section, an initial PSF is generated by averaging all the reference PSFs. We then use a downhill simplex algorithm to optimize the contribution from each PSF image, searching for the combination which provides the best fit to the target image. This optimization is done on several sections simultaneously (in a region 3 sections in radius and 2 sections in angle) to minimize the probability of the algorithm artificially subtracting out real companions. After optimization in the large region, only the central section is output to the final PSF. This provides smooth transitions between adjacent PSF sections because they share many of the image pixels used for the optimization.

This procedure is iterated across all the sections of the image, producing a PSF which is an optimal local combination of the reference PSFs and which can then be subtracted from the target star's PSF. The PSF subtraction typically leaves residuals that are consistent with photon noise only (for these relatively short exposures). Figure 3 shows an example of the PSF subtraction performance.

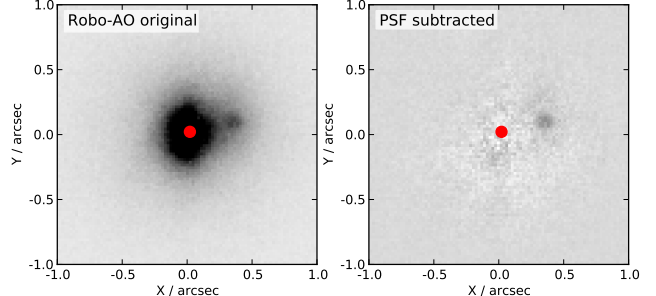


FIG. 3.— A typical Robo-AO target before and after PSF subtraction using the locally-optimized ensemble of PSF references described in the text.

### 3.3. Automated Companion Detection and Imaging Performance Metrics

We developed a new automated companion detection algorithm for Robo-AO data, based on the radially-varying noise profiles in the PSF-subtracted images. To search for targets which could affect the *Kepler* light curves we limited the detection radius of this initial search to a 2.5' radius from the target KOIs. We first measure the local image noise as a function of distance from the target star, by covering the PSF-subtracted target image with 4-pixel-diameter apertures and measuring the RMS of the pixel values in each aperture, along with the average PSF-subtraction residual signal. We then fit a quadratic to interpolate the changes in noise and residual values as a function of radius from the target star position. For each pixel in the PSF-subtracted image we then use the noise and residual fits to estimate the

significance of that pixel's signal level. This procedure generates a significance image where bright pixels in regions of high photon noise (i.e. in the core of the star) are down-weighted compared to those in lower-noise areas.

The significance image yields the pixels which have some chance of denoting detections of stars, but does not take into account the shapes of the detections – a single bright pixel surrounded by insignificant pixels is more likely to be due to a cosmic ray hit than a stellar companion, and a tens-of-pixels-wide blob is likely due to imperfect PSF subtraction. We quantify this by correlating the significance image by a Gaussian corresponding to the diffraction limit of the Robo-AO observation. We then select the pixels which show the most significant detections ( $> 5\sigma$ ) as possible detections, and amalgamate groups of multiple significant pixels into single detections.

After automated companion detection we also manually checked each image for companions, to check the performance of the automated system and to search for faint but real companions which could have been fit and removed by spurious speckles in the PSF references. The automated system picked up every manually-flagged companion, and had a 3.5% false-positive rate from all the images, mainly due imperfect PSF subtraction.

We evaluated the contrast-vs.-radius detection performance of the PSF-subtraction and automated companion detection code by performing Monte-Carlo companion-detection simulations. The time-consuming simulations could only be performed on a group of representative targets, and so we established a quantitative image quality metric that allows each of our observations to be tied into the contrast curves for a particular test target. We first parametrized the performance of each observation of our dataset by fitting a two-component model to the PSF based on two Moffat functions tuned to separately measure the widths of the core and halo of the PSF. We then picked the 12 single-star observations to represent the variety of PSF parameter space in our dataset. For each test star, we added a simulated companion into the observation at a random separation, position angle and contrast, ran the PSF subtraction and automated companion detection routines, and measured the detection significance (if any) of the simulated companion. We repeated this for 1000 simulated companions<sup>8</sup>. We then binned the simulated detections as a function of separation from the target star, and in each radial bin fit a linear significance-vs.-contrast relation. We use the intersection of the fitted relation with a  $5\sigma$  detection to provide the minimum-detectable contrast in each radial bin.

We found that the PSF core size was an excellent predictor of contrast performance, while the halo size did not affect the contrast significantly. The halo is effectively removed by the PSF subtraction, and the contrast is thus chiefly limited by the companion SNR, which scales with the achieved PSF core size (rather than the image FWHM, which we found is a weak predictor of contrast performance in Robo-AO data). On this basis we use the

<sup>8</sup> For each simulated companion PSF we removed the central spike introduced by photon-noise-limited observations by averaging with nearby pixels (Law et al. 2006a,b, 2009); this conservative correction reduces our claimed detectable contrast by up to 25%.

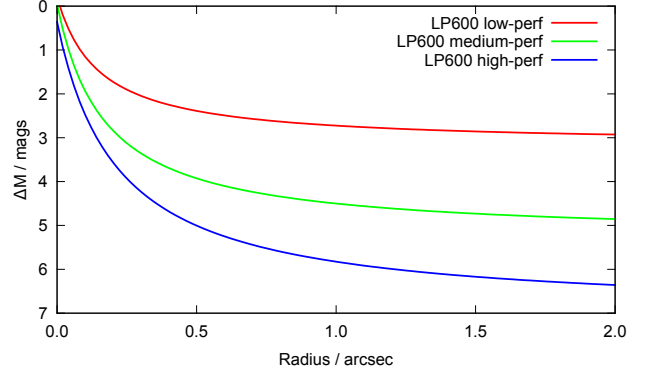


FIG. 4.— Monte-Carlo contrast ratios for three representative targets observed in the LP600 filter.

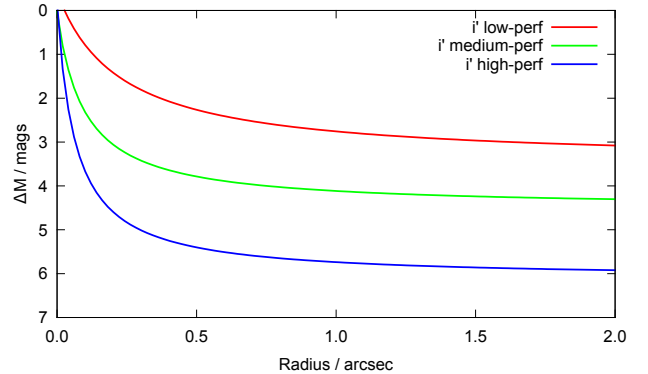


FIG. 5.— Monte-Carlo contrast ratios for three representative targets observed in the SDSS-i filter.

PSF core size to assign targets to contrast-performance groups (low, medium and high). As the imaging performance degrades, we found that the relative contribution of the fitted core PSF decreases, while the core itself shrinks. The somewhat counter-intuitive size decrease is because poor imaging quality inevitably corresponds with poor SNR on the tip/tilt measurements, which leads to the frame alignments locking onto photon noise spikes, and thus a single-pixel-sized spike in the images (Law et al. 2006a, 2009). Images with a diffraction-limited-sizes core ( $\sim 0.^{\circ}15$ ) are assigned to the high-performance groups; smaller cores, where the imaging performance is degraded, were assigned to the lower-performance groups.

Figures 4 and 5 show the contrast curves resulting from this procedure, for clarity smoothed with fitting functions of form  $a - b/(r - c)$  (where  $r$  is the radius from the target star). The i-band observations obtain better contrast close-in than the LP600 filter, because of their improved Strehl ratios, while the LP600 filter allows somewhat improved contrast at wider radii. Over all the observations, there were 154 targets in the low-performance category, 364 in the medium category and 197 in the high-performance group.

### 3.4. Companion characterization

We measured the contrast ratios, position angles and projected separations of the detected companions using the PSF-subtracted images. We measured the pixel position of the companion relative to the primary star by centroiding a region around the core of each star using

the pre-PSF-subtraction images for the primary. We determined the contrast ratio in two ways: for the widest separations aperture photometry on the original images, and for the closer systems separated aperture photometry measuring the ratio between the companion light in the PSF-subtracted images determined in Section 3.2 and the primary light in images with the companion subtracted out using the PSF estimates. In all cases the aperture sizes were optimized for the system separation and the available signal.

The locally-optimized PSF subtraction will attempt to remove flux associated with companions by using other PSFs with (non-astrophysical) excess brightness in those areas, because it is trying to achieve the best fit to the target images without discrimination between real companions and speckles. By selecting an optimization over a region containing many PSF core sizes, we reduce the algorithm’s ability to subtract away companion light for detection purposes. However, the companion will still be artificially faint in PSF-subtracted images, leading to errors in flux ratio measurements. To avoid this we re-run the PSF fit excluding a 6-pixel-diameter region around any detected companion. The PSF-fit regions are large enough to provide a good estimate for the PSF underneath the companion, and the companion brightness is not artificially reduced by this procedure. Finally, we verified the measured positions and contrast ratios in direct measurement from non-PSF-subtracted images.

We calculated the contrast ratio uncertainty on the basis of the difference between the injected and measured contrasts of the fake companions injected during the contrast-curve calculations (§3.3). We found that the detection significance of the companion was the best predictor of the contrast ratio accuracy, and so we use a fit to that relation to estimate the contrast ratio uncertainty for each companion. We note that the uncertainties are much higher than would be naively expected from the SNR of the companion detection, as they include an estimate of the systematic errors resulting from the AO imaging, PSF-subtraction and contrast-measurement processes. We calculated the underuncertainties of the companion separation and position angles using estimated systematic errors in the position measurements, depending on the separation of the companion, and included the an estaimte of the maximal changes in the Robo-AO orientation throughout the observation period.

#### 4. DISCOVERIES

We resolved 53 *Kepler* planet candidate hosts into multiple stars; the discovery images are summarized in Figure 6 and the separations and contrast ratios are shown in figure 7. The measured companion (§5 addresses the probability of physical association for these objects) properties are detailed in Table 2 (secure detections at high confidence levels) and Table 3 (less-secure detections of faint or very close objects where there is a chance one of two of the targets could be false positives).

Two of the targets showed potential companions that were not well-resolved by Robo-AO but were suggestive of interesting companions. KOI-1962 showed PSF-core-elongation indicative of a  $<0.15$ -separation nearly-equal-contrast binary. KOI-1964 has a probable faint companion at a separation of  $0''.4$ ; dynamic speckle noise re-

duces the detection significance to  $\approx 3\sigma$ . We confirmed the Robo-AO detections with NIRC2-NGS (Wizinowich et al. 2000) on Keck II on 23 July 2013 (Figure 8).

#### 4.1. Lower-confidence Detections

A number of additional probable companions fell just below our formal  $5\sigma$  detection criteria and are listed in table 3. We consider these very likely to be real (indeed, three have been previously detected by other groups), but in the present data we cannot exclude the possibility that one or two of these detections are spurious speckles.

#### 4.2. Comparison to other surveys

Lillo-Box et al. (2012) (hereafter LBB12) observed 98 KOIs using a Lucky Imaging system. Seven of the targets for which they discovered companions within a  $2.5$  arcsecond radius are also in our survey. Both surveys detect KOI-401 at a separation of  $2.0$  arcseconds and a contrast of  $2.6$  magnitudes (LBB12 i-band) or  $2.9$  magnitudes (Robo-AO LP600). The companions to KOI-628 were visible in our survey but at contrasts that placed them in the “likely detections” group. LBB12 detected a companion to KOI-658 at  $1''.9$  radius and a contrast of  $4.6$  magnitudes in i-band. At that radius for the performance achieved on KOI-658 the Robo-AO snapshot-survey limiting contrast ratio is  $\sim 4.0$  magnitudes and so we do not re-detect that companion. For the same reason we also do not re-detect the companions to KOI-703 ( $6.4$  magnitudes contrast), KOI-704 ( $5.0$  magnitudes contrast) and KOI-721 ( $3.9$  magnitudes contrast). The  $0.13$  arcsecond-radius companion to KOI-1537 detected in Adams et al. (2013) is at too close a separation to be detectable in our survey. The LBB12 companion to KOI-1375 is visible in our dataset, but has a contrast ratio of  $4.0$  magnitudes, under our formal detection limit and well below the  $2.75$  magnitude i-band contrast measured by LBB12. The target is not strongly coloured according to LBB12 and it is not obvious why the companion is so much fainter in our survey.

## 5. DISCUSSION

### 5.1. Implications for *Kepler* Planet Candidates

The detection of a previously unknown star within the photometric aperture of a KOI host star will affect the derived radius of any planet candidate around that host star, because the *Kepler* observed transit depth is shallower than the true depth due to dilution. The degree of this effect depends upon the relative brightness of the target and secondary star, and which star is actually being transited. In particular, if there is more than one star in the photometric aperture and the transiting object is around a star that contributes a fraction  $F_i$  to the total light in the aperture, then

$$\delta_{\text{true}} = \delta_{\text{obs}} \left( \frac{1}{F_i} \right), \quad (1)$$

where  $\delta_{\text{true}}$  is the true intrinsic fractional transit depth and  $\delta_{\text{obs}}$  is the observed, diluted depth. Since  $\delta \propto (R_p/R_*)^2$ , the true planet radius in the case where the transit is around star  $i$  is

$$R_{p,i} = R_{*,i} \left( \frac{R_p}{R_*} \right)_0 \sqrt{\frac{1}{F_i}}, \quad (2)$$

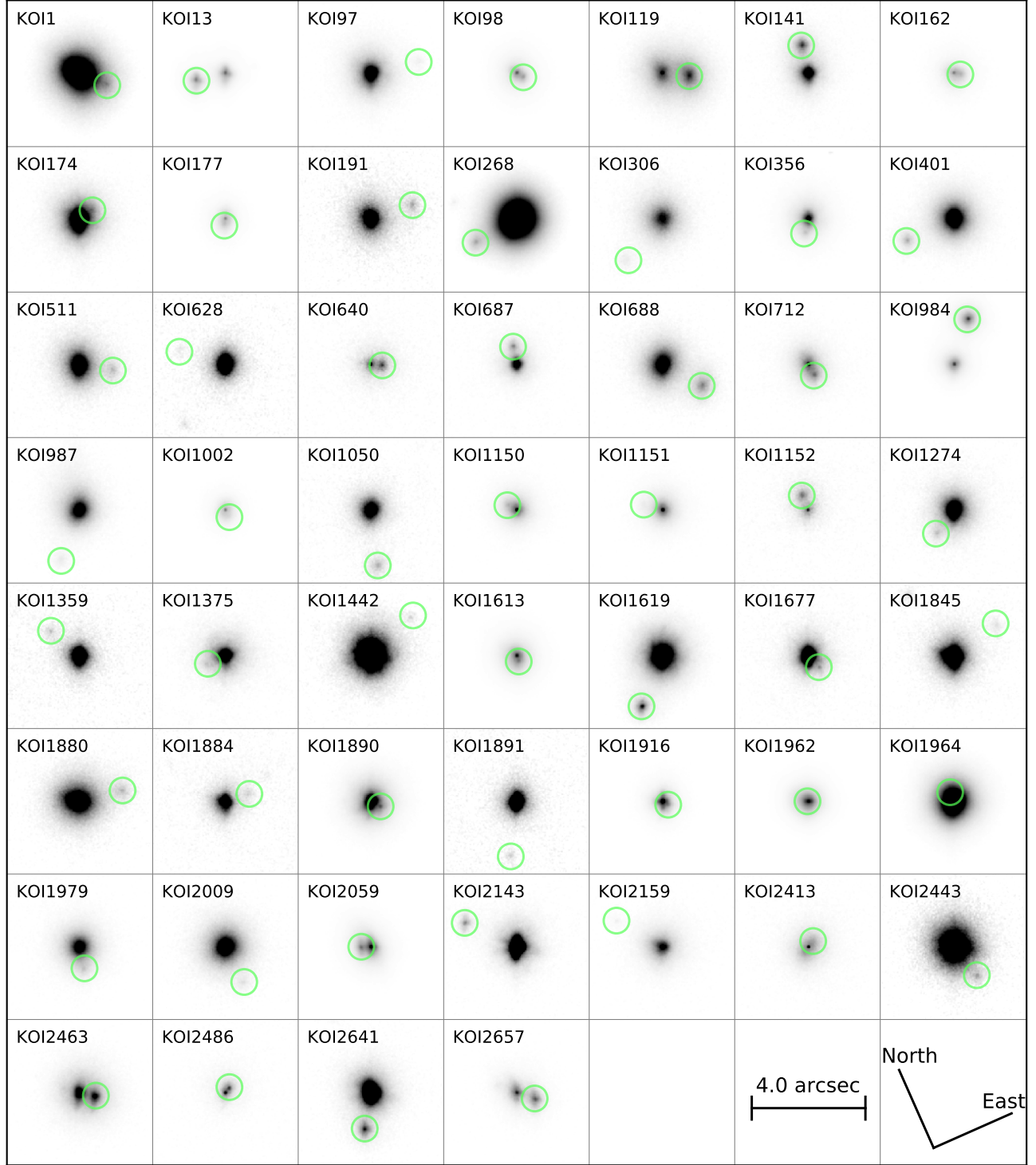


FIG. 6.— The *Kepler* planet candidates resolved into multiple stars by Robo-AO. The grayscale of each 4'' cutout is selected to show the companion; the angular scale and orientation is identical for each cutout.

TABLE 2  
SECURE DETECTIONS OF OBJECTS WITHIN 2''.5 OF *Kepler* PLANET CANDIDATES

KOI	$m_i$	Obs.date	Filter	Signf.	Separation	PA	Contrast	Previous detection?
KOI-1	11.168	2012/07/16	i	13	1.13±0.06	135±2	3.95±0.33	
KOI-13	10.548	2012/10/06	i	950	1.16±0.06	279±2	0.19±0.06	A12
KOI-98	12.024	2012/07/17	i	80	0.29±0.06	140±6	0.10±0.16	B11, H11, A12, H12
KOI-119	12.452	2012/07/16	i	38	1.05±0.06	118±2	0.87±0.22	
KOI-141	13.441	2012/07/18	i	34	1.10±0.06	11±2	1.39±0.23	A12
KOI-162	13.626	2012/07/18	LP600	19	0.29±0.06	117±7	0.81±0.29	
KOI-174	13.449	2012/07/18	LP600	7	0.60±0.06	77±3	4.43±0.44	A13
KOI-177	12.979	2012/07/18	i	12	0.24±0.06	215±8	0.97±0.35	
KOI-191	14.747	2012/09/01	LP600	5	1.69±0.06	94±2	3.09±0.49	
KOI-268		2012/09/14	LP600	23	1.81±0.06	265±2	3.82±0.27	A12
KOI-356	13.532	2012/07/28	LP600	17	0.56±0.06	218±4	2.92±0.30	
KOI-401	13.729	2012/08/05	LP600	19	1.99±0.06	268±2	2.90±0.29	L12, B13
KOI-511	14.017	2012/09/01	LP600	7	1.28±0.06	123±2	3.33±0.43	
KOI-640	13.058	2012/07/28	i	16	0.44±0.06	117±4	0.62±0.31	
KOI-687	13.613	2012/08/04	i	21	0.70±0.06	13±3	2.04±0.28	
KOI-688	13.849	2012/09/14	LP600	19	1.71±0.06	141±2	2.19±0.29	
KOI-712	13.51	2012/08/05	i	21	0.47±0.06	173±4	1.17±0.28	
KOI-984	11.353	2012/08/03	i	120	1.80±0.06	42±2	0.01±0.14	
KOI-1002	13.362	2012/08/03	i	9	0.30±0.06	173±6	2.31±0.38	
KOI-1050	13.696	2012/08/03	i	8	2.09±0.06	197±2	2.70±0.40	
KOI-1150	13.139	2012/08/05	i	9	0.39±0.06	322±5	2.41±0.39	
KOI-1152	13.622	2012/09/14	LP600	16	0.59±0.06	2±3	0.31±0.31	
KOI-1274	13.107	2012/08/06	i	7	1.10±0.06	241±2	3.75±0.44	
KOI-1613		2012/08/29	i	36	0.22±0.06	184±9	1.30±0.22	
KOI-1619	11.427	2012/08/29	i	60	2.10±0.06	226±2	2.82±0.18	
KOI-1677	14.073	2012/09/04	LP600	7	0.61±0.06	159±3	4.76±0.44	
KOI-1880	13.835	2012/07/15	LP600	6	1.70±0.06	100±2	3.66±0.45	
KOI-1890	11.555	2012/08/29	i	42	0.41±0.06	142±5	3.44±0.21	
KOI-1916	13.42	2012/09/13	LP600	31	0.27±0.06	143±7	2.73±0.24	
KOI-1962		2012/08/30	i	...	0.12	...	0.04 (K <sub>s</sub> )	
KOI-1964	10.5	2012/08/30	i	...	0.39	...	1.9 (K <sub>s</sub> )	
KOI-1979	12.786	2012/08/30	i	9	0.84±0.06	192±3	3.20±0.39	
KOI-2059	12.558	2012/10/06	LP600	120	0.38±0.06	291±5	1.10±0.14	
KOI-2143	13.872	2012/10/06	LP600	19	2.16±0.06	317±2	3.50±0.29	
KOI-2463	12.609	2012/08/31	i	70	0.62±0.06	125±3	0.75±0.17	
KOI-2486	12.89	2012/08/31	i	18	0.24±0.06	63±8	0.49±0.30	
KOI-2641	13.63	2012/10/06	LP600	36	1.42±0.06	214±2	2.56±0.22	
KOI-2657	12.655	2012/10/06	LP600	62	0.73±0.06	131±3	0.27±0.18	

References for previous detections are denoted with the following codes: Adams et al. 2012 (A12); Adams et al. 2013 (A13); Barrado et al. 2013 (B13); Buchhave et al. 2011 (B11); Horch et al. 2012; Howell et al. 2011 (H11); Lillo-Box et al. 2012 (L12); Narita et al. 2010 (N10).

TABLE 3  
LIKELY DETECTIONS OF OBJECTS WITHIN 2''.5 OF *Kepler* PLANET CANDIDATES

KOI	$m_i$	Obs.date	Filter	Signf.	Separation	PA	Contrast	Previous detection?
KOI-97	12.724	2012/07/17	i	4.2	1.90±0.06	99±2	4.61±0.52	A12
KOI-306	12.363	2012/07/18	i	3.6	2.06±0.06	243±2	4.16±0.56	A12
KOI-628	13.744	2012/08/03	i	1.4	1.83±0.06	309±2	5.20±0.80	L12, B13
KOI-987	12.327	2012/08/03	i	2.4	2.05±0.06	225±2	4.10±0.66	
KOI-1151	13.198	2012/08/05	i	3.2	0.75±0.06	309±3	3.49±0.58	
KOI-1359	15.025	2012/09/04	LP600	3.4	1.43±0.06	333±2	3.80±0.57	
KOI-1375	13.533	2012/08/06	i	4.0	0.77±0.06	269±3	4.38±0.53	
KOI-1442	12.296	2012/08/06	i	3.3	2.24±0.06	70±2	6.68±0.57	
KOI-1845	14.05	2012/09/13	LP600	2.9	2.06±0.06	77±2	4.97±0.60	
KOI-1884	15.158	2012/09/13	LP600	2.5	0.95±0.06	96±2	3.65±0.64	
KOI-1891	14.957	2012/09/13	LP600	3.0	2.09±0.06	210±2	4.46±0.60	
KOI-2009	13.616	2012/09/14	LP600	4.9	1.51±0.06	176±2	4.11±0.49	
KOI-2159	13.293	2012/08/31	i	4.0	2.00±0.06	323±2	3.99±0.53	
KOI-2413	14.684	2012/09/14	LP600	2.4	0.31±0.06	67±6	2.11±0.66	
KOI-2443	13.83	2012/10/06	LP600	3.7	1.39±0.06	163±2	5.37±0.55	

References for previous detections are denoted with the following codes: Adams et al. 2012 (A12); Barrado et al. 2013 (B13); Lillo-Box et al. 2012 (L12).

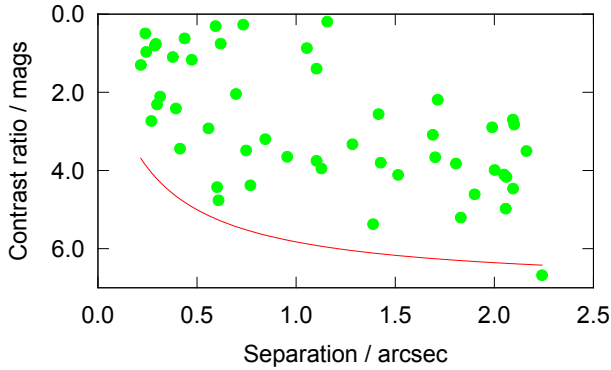


FIG. 7.— The separations and contrast ratios of the detected companions compared to the survey’s typical high-performance contrast curve (one very faint companion was detected around a bright KOI in exceptional conditions). The distribution of companion properties has no evidence for unaccounted incompleteness effects, although there is an excess of bright companions at close separations, suggesting that those companions are more likely to be physically associated.

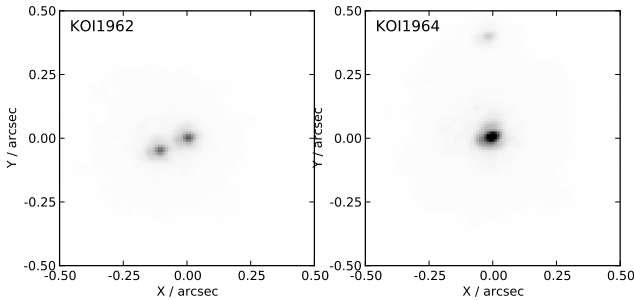


FIG. 8.— Keck-AO NIRC2 J-band images confirming two Robo-AO companion detections.

where  $R_{\star,i}$  is the radius of star  $i$ , and the 0 subscript represents the radius ratio implied by the diluted transit, or what would be inferred by ignoring the presence of any blending flux.

Thus, for each planet candidate in KOI systems observed to have close stellar companions, the derived planet radius must be corrected—and there are two potential scenarios for each candidate: the eclipsed star is either star A (the brighter target star) or star B (the fainter companion).

In case A, the corrected planet radius is

$$R_{p,A} = R_{p,0} \sqrt{\frac{1}{F_A}}, \quad (3)$$

and in case B,

$$R_{p,B} = R_{p,0} \frac{R_B}{R_A} \sqrt{\frac{1}{F_B}}. \quad (4)$$

Case A is straightforward, with nothing needed except the observed contrast ratio (in order to calculate  $F_A$ ). Case B, however, in addition to needing  $F_B$ , needs also the ratio  $R_B/R_A$ . If the observed companion is an unassociated background star, then the single-band Robo-AO observation does not constrain  $R_B$ . However, under the assumption that the companion is physically bound, then we can estimate its type, given assumed knowledge about the primary star A.

In order to accomplish this, we use the Dartmouth stellar models (Dotter et al. 2008) and the measured primary KOI star properties listed in the NASA Exoplanet Archive. For the mass and age of the primary, we use the Dartmouth isochrones to find an absolute magnitude in the observed band (approximating the LP600 bandpass as *Kepler* band), then we inspect the isochrone to find the mass of a star that is the appropriate amount fainter (according to the observed contrast ratio), and assign the stellar radius  $R_B$  accordingly.

Table 4 summarizes how the planet radii change under both case A and B for each KOI in all the systems in which we detect companions. We also list an additional case  $B_{bg}$  for the situation in which the eclipsed star is not physically bound—since we do not have a constraint on  $R_B$  in this situation, we simply list the planet radii for the case of  $R_B = 1M_\odot$ , which allows for simple scaling.

Interestingly, under case B where the transit is assumed to be around a bound companion, in many cases the implied planet radius is not indicative of a false positive. This is because in order to get a large radius correction there must be a large contrast ratio, which then (in the physically associated scenario) implies that the secondary is a small star, which shrinks the radius correction factor. In fact, the only candidates which attain clearly non-planetary radii under case B are those which already have radii comparable to or larger than Jupiter to begin with. On the other hand, case  $B_{bg}$  often suggests a non-planetary radius, as the stellar radius in this case is not bound to shrink as the contrast ratio grows.

## 5.2. Particularly interesting systems

There are several KOIs with detected companions that we note as being of particular interest.

### 5.2.1. KOI-191: A probable “coincident multiple”

KOI-191 was identified by Batalha et al. (2013a) to have four planet candidates, with periods of approximately 0.7, 2.4, 15.4, and 38.7 days. The 15.4d candidate has an estimated radius of  $11 R_\oplus$ , whereas all the rest are smaller than  $1.5 R_\oplus$ . This system is notable because in the entire cumulative KOI catalog, there are only four multi-candidate systems that have a planet candidate (either CANDIDATE or NOT DISPOSITIONED on the NEA) with  $10R_\oplus < R < 20R_\oplus$  and  $P < 20$ d. Two of these four (KOI-199 and KOI-3627) are marked as 2-planet systems but the second candidate in each is identified as a FP in the Q1-Q12 activity table, making them effectively single-candidate systems. And the host star of KOI-338 has  $R_\star = 19.2$ , and its two candidates have radii of 17 and  $37 R_\oplus$ , making that system most likely a stellar multiple system. This leaves KOI-191 as the only multiple-candidate *Kepler* system including a Jupiter-like candidate with  $P < 20$ d. By contrast, there are 62 single candidates that match these same radius and period cuts (64 including KOI-199 and KOI-3627).

Based on the apparent rarity of planetary systems with this architecture and the fact that we detect a stellar companion to the KOI-191 host star, we conclude that this is a likely “coincident multiple” system, with KOI-191.01 around one of the stars, and the other three around the other. There are three possibilities: 1) Since the companion star (1.<sup>69</sup> separation) is 3.1 mag fainter,

TABLE 4  
IMPLICATIONS ON DERIVED RADIUS OF *Kepler* PLANET CANDIDATES

KOI	$P$ [d]	$R_p$ [ $R_\oplus$ ]	$R_\star$	$\Delta m$	sep	$R_{\star,B}$	$R_{p,A}$	$R_{p,B}$	$R_{p,B_{bg}}$
1.01	2.471	14.40	1.06	4.0	1.13	0.50	14.6	42.0	84.9
13.01	1.764	23.00	2.70	0.2	1.16	2.70	31.2	34.0	12.6
97.01	4.885	16.10	1.78	4.6	1.90	0.57	16.2	43.6	76.1
98.01	6.790	10.00	1.63	0.8	0.29	1.26	12.2	13.4	10.7
119.01	49.184	3.90	0.94	0.9	0.10	0.76	4.7	5.6	7.5
119.02	190.313	3.40	—	—	—	—	4.1	4.9	6.5
141.01	2.624	5.43	0.93	1.4	1.10	0.72	6.1	9.0	12.5
162.01	14.006	2.54	0.96	0.8	0.29	0.79	3.1	3.7	4.7
174.01	56.354	1.94	0.63	4.4	0.60	0.21	2.0	5.1	24.0
177.01	21.060	1.84	1.06	1.0	0.24	0.84	2.2	2.7	3.2
191.01	15.359	11.00	0.88	3.1	1.69	0.55	11.3	29.3	53.4
191.02	2.418	2.30	—	—	—	—	2.4	6.1	11.2
191.03	0.709	1.24	—	—	—	—	1.3	3.3	6.0
191.04	38.652	2.30	—	—	—	—	2.4	6.1	11.2
268.01	110.379	1.73	0.79	3.8	1.81	0.33	1.8	4.3	13.0
306.01	24.308	2.29	0.87	4.2	2.06	0.39	2.3	7.0	18.0
356.01	1.827	5.73	1.60	2.9	0.56	0.66	5.9	9.4	14.2
401.01	29.199	7.23	1.58	2.9	1.99	0.66	7.5	11.9	18.0
401.02	160.017	7.31	—	—	—	—	7.6	12.0	18.2
401.03	55.328	2.66	—	—	—	—	2.8	4.4	6.6
511.01	8.006	2.80	1.08	3.3	1.28	0.61	2.9	7.5	12.3
511.02	4.264	1.58	—	—	—	—	1.6	4.2	6.9
628.01	14.486	3.10	1.29	5.2	1.83	0.38	3.1	10.1	26.5
640.01	30.996	2.44	0.89	0.6	0.44	0.80	3.1	3.6	4.5
687.01	4.178	1.46	0.93	2.0	0.70	0.64	1.6	2.8	4.3
688.01	3.276	2.28	1.35	2.2	1.71	0.77	2.4	3.8	4.9
712.01	2.178	1.08	0.84	1.2	0.47	0.76	1.3	1.9	2.6
984.01	4.287	3.19	0.92	0.0	1.80	0.92	4.5	4.5	4.9
987.01	3.179	1.28	0.92	4.1	2.05	0.42	1.3	3.9	9.3
1002.01	3.482	1.36	1.01	2.3	0.30	0.66	1.4	2.7	4.1
1050.01	1.269	1.40	0.76	2.7	2.09	0.46	1.5	3.1	6.6
1050.02	2.853	1.40	—	—	—	—	1.5	3.1	6.6
1150.01	0.677	1.10	1.09	2.4	0.39	0.66	1.2	2.1	3.2
1151.01	10.435	1.46	0.97	3.5	0.75	0.50	1.5	3.8	7.7
1151.02	7.411	1.15	—	—	—	—	1.2	3.0	6.0
1151.03	5.249	0.70	—	—	—	—	0.7	1.8	3.7
1152.01	4.722	19.56	0.65	0.3	0.59	0.54	25.9	24.9	45.7
1274.01	362.000	4.73	0.79	3.8	1.10	0.37	4.8	12.6	34.3
1359.01	37.101	3.50	0.92	3.8	1.43	0.58	3.6	13.0	22.2
1359.02	104.820	7.30	—	—	—	—	7.4	27.1	46.3
1375.01	321.214	6.78	1.17	4.4	0.77	0.50	6.8	22.0	44.0
1442.01	0.669	1.23	1.00	6.7	2.24	0.20	1.2	5.2	26.8
1613.01	15.866	1.07	1.04	1.3	0.22	0.78	1.2	1.7	2.1
1619.01	20.666	0.80	0.62	2.8	2.10	0.33	0.8	1.6	4.9
1677.01	52.070	2.18	0.85	4.8	0.61	0.43	2.2	9.8	23.1
1677.02	8.512	0.81	—	—	—	—	0.8	3.7	8.6
1845.01	1.970	1.50	0.70	5.0	2.06	0.19	1.5	4.0	21.2
1845.02	5.058	21.00	—	—	—	—	21.1	56.2	297.4
1880.01	1.151	1.49	0.52	3.7	1.70	0.18	1.5	2.8	15.6
1884.01	23.120	5.00	0.92	3.6	0.95	0.55	5.1	16.3	29.7
1884.02	4.775	2.63	—	—	—	—	2.7	8.6	15.6
1890.01	4.336	1.50	1.32	3.4	0.41	0.62	1.5	3.5	5.7
1891.01	15.955	1.85	0.69	4.5	2.09	0.33	1.9	6.9	21.1
1891.02	8.260	1.26	—	—	—	—	1.3	4.7	14.4
1916.01	20.679	2.16	0.96	2.7	0.27	0.67	2.2	5.5	8.2
1916.02	9.600	1.89	—	—	—	—	2.0	4.8	7.2
1916.03	2.025	0.92	—	—	—	—	1.0	2.4	3.5
1979.01	2.714	1.13	0.94	3.2	0.84	0.52	1.2	2.8	5.4
2009.01	86.749	2.20	0.97	4.1	1.51	0.48	2.2	7.3	15.2
2059.01	6.147	0.83	0.67	1.1	0.38	0.60	1.0	1.4	2.4
2143.01	4.790	1.14	0.81	3.5	2.16	0.54	1.2	3.9	7.2
2159.01	7.597	1.07	0.88	4.0	2.00	0.48	1.1	3.8	7.7
2159.02	2.393	0.99	—	—	—	—	1.0	3.5	7.2
2413.01	12.905	1.32	0.65	2.1	0.31	0.46	1.4	2.7	5.8
2413.02	31.200	1.26	—	—	—	—	1.3	2.6	5.5
2443.01	6.792	1.20	1.09	5.4	1.39	0.41	1.2	5.3	13.1
2443.02	11.837	1.02	—	—	—	—	1.0	4.5	11.1
2463.01	7.467	1.02	0.97	0.8	0.62	0.94	1.2	1.7	1.8
2486.01	4.268	2.71	1.17	0.5	0.24	1.08	3.5	4.0	3.7
2641.01	3.556	1.20	1.10	2.6	1.42	0.66	1.3	2.5	3.7
2657.01	5.224	0.60	0.80	0.3	0.73	0.89	0.8	1.0	1.1

if it is the host of KOI-191.01, then it is most likely a stellar eclipsing binary; 2) if the primary star hosts .01, then the secondary likely hosts the three-candidate system, in which case .02-.04 are more likely all super-Earth/Neptune-sized; 3) it may be the case that all four planets are indeed around the same star, which would make KOI-191 a planetary system of unusual architecture, inviting further study.

#### 5.2.2. KOI-268: Habitable Zone Candidate?

KOI-268 hosts a planet candidate in a 110-d orbit. The candidate has a radius of  $1.7 R_{\oplus}$  and an equilibrium temperature of 295 K, according to the NEA. However, Robo-AO detects a stellar companion 3.8 mag fainter at a separation of  $1''.81$ . We also note the presence of a possible fainter companion at a  $2.45''$  separation, a position angle of  $306^\circ$  and a contrast ratio of  $\approx 5.5$  magnitudes. The equilibrium temperature calculation of the candidate is based on the estimated effective temperature of the host star and the planet is therefore unlikely to be in the habitable zone if it is around one of the companions.

#### 5.2.3. KOI-628

KOI-628 has a previously-detected faint companion at a separation of  $1''.83$  (Barrado et al. 2013; Lillo-Box et al. 2012). We also re-detect a further possible companion just beyond our detection-target radius, at  $2.55$  separation.

#### 5.2.4. KOI-1151: Another possible coincident multiple

KOI-1151, discovered by this survey to have a companion with  $\Delta i \approx 3.5$  at a separation of  $0''.75$ , is another system with unusual architecture that might be best explained if the candidates were shared between the two stars. This system has 5 detected planet candidates, with periods of 5.25, 7.41, 10.44, 17.45, and 21.72 days.<sup>9</sup> What makes this system appear unusual is the presence of the 7.41d candidate in between the 5.25d and 10.44d candidates, which have nearly exact 2:1 commensurability. Of the 22 multi-KOI systems that have a pair of planets within 2% of exact 2:1 commensurability, only KOI-1151 and KOI-2038 have another candidate between the pair (the inner two planets in this system have been confirmed via transit timing variations by Ming et al. 2013). Migration can tend to deposit planets in or near resonant configurations, but it appears to be unusual for a planet to be stuck between two other planets that are near a strong resonance—perhaps this is an indication that the KOI-1151 system is not a single planetary system at all, but rather two separate systems. Another plausible configuration is that KOIs 1151.02 (the interloper at 7.41d) and 1151.05 (the 21.72d candidate) are separated from the other three as those two are near 3:1 commensurability.

#### 5.2.5. KOI-1442: Largest contrast-ratio companion

We detect a likely companion to KOI-1442 (*Kepler* magnitude of 12.52) at a separation of  $2''.24$  and a contrast ratio of  $\sim 6.7$ . KOI-1442.01 is a planet candidate

with a period of 0.67d and a radius of  $1.2 R_{\oplus}$ ; however, the detection of this companion, which is likely to be a background source, means that if it were the source of the signal, the radius of the companion would be  $\sim 20\times$  larger (if the background source is the same radius as KOI-1442). Especially since there are hints that very short-period systems may be more likely to be blended binaries (Colón et al. 2012), there might be concern that this candidate is a background eclipsing binary false positive. However, against this hypothesis stands the centroid offset analysis of Bryson et al. (2013) as presented on the NEA, which suggests that the source of the transit could be at most maybe  $0''.5$  away from the target position. Therefore, while this system is notable due to the faintness of its detected companion, the companion is unlikely to be the source of a false positive due to its large separation.

#### 5.2.6. KOI-1845: One likely false positive in a two-candidate system

KOI-1845 hosts two planetary candidates: .01 is a  $1.5 R_{\oplus}$  candidate in a 1.97-d orbit, and .02 is a  $21 R_{\oplus}$  candidate in a 5.06-d orbit. Without any AO observations this system would be suspicious because close-in giant planets are very unlikely to have other planets nearby (see §5.2.1); in addition, candidate .02 has a very large *Kepler*-estimated radius and appears to have a significantly V-shaped transit. In this survey we detect a companion 5.0 mag fainter at a separation of  $2''.06$ , and suggest that the most likely explanation for KOI-1845.02 is that this companion is a background eclipsing binary.

#### 5.2.7. Systems with secure small planets

There are five systems that host planet candidates with  $R_p < 2R_{\oplus}$  in which we have detected stellar companions but whose interpretation as small planets ( $< 2R_{\oplus}$ ) is nonetheless secure, as long as the companions are physically bound. This happens when the candidates are small and the companion is of comparable brightness such that the potential effect of dilution is minimized, even if the eclipse is around the fainter star. The specifics of these systems can be seen in Table 4 but we call attention to them here: KOI-1613, KOI-1619, KOI-2059, KOI-2463, and KOI-2657.

### 5.3. Stellar Multiplicity and Kepler Planet Candidates

Our detection of 53 planetary candidates with nearby stars from 715 targets implies an overall multiplicity rate of  $7.4\%\pm 1.0\%$ . In this section we search for broad-scale changes in stellar multiplicity with planetary candidate properties. The companions we detect may not be physically bound, nor are we sensitive to binaries in all possible orbital locations around these KOIs. This multiplicity rate, therefore, should not be expected give a full description of multiplicity around *Kepler* planet candidates; however, we can use the current survey results to compare the multiplicity rates of different populations of planet candidates. Future papers from the ongoing Robo-AO survey will investigate the multiplicity properties of *Kepler* candidates in more detail, including quantifying the effects of association probability and incompleteness.

<sup>9</sup> The NEA cumulative KOI table gives KOI-1151.01 a 5.22-d period rather than a 10.44, which would be clearly unphysical in the presence of another candidate with a 5.25-d period; the Q1-Q12 table corrects the period of 1151.01 to 10.44.

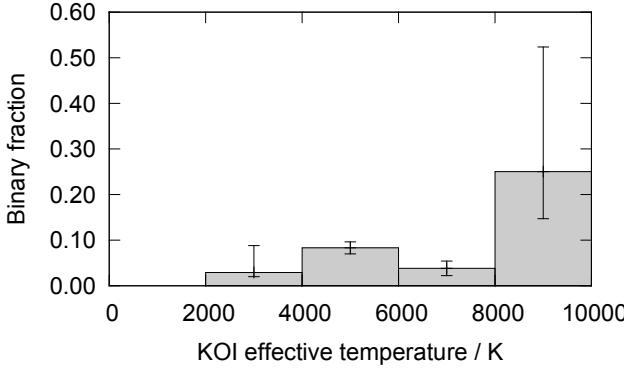


FIG. 9.— The fraction of KOIs with detected nearby stars as a function of stellar effective temperature.

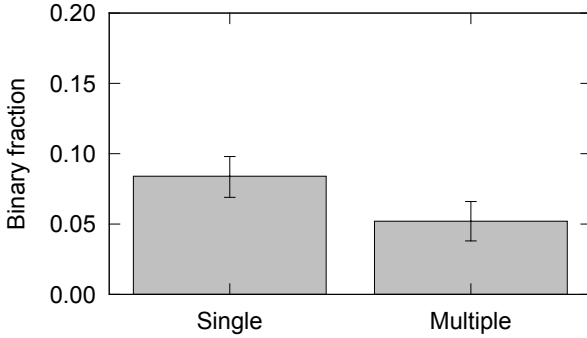


FIG. 10.— The binarity fractions of KOIs hosting single and multiple detected planetary systems.

### 5.3.1. Stellar multiplicity rates vs. host-star temperature

Figure 9 shows the fraction of multiple stellar systems around *Kepler*-detected planetary systems as a function of stellar temperature from the *Kepler* Input Catalog (Brown et al. 2011). We do not detect any significant change in the stellar multiplicity fraction with KOI temperature, although the initial survey presented here does not cover a large number of non-solar-type stars.

### 5.3.2. Stellar multiplicity and multiple-planet systems

It is expected that multiple-planet systems detected by *Kepler* are less likely to be false positives than single-planet systems because there are far fewer false-positive scenarios which can lead to multiple-period false-positives. In Figure 10 we show the stellar multiplicity rates for single and multiple planet detections. There is a difference in stellar multiplicity between the single and multiple planet detections, but with only  $1.6\sigma$  significance, suggesting that at least in the current dataset we cannot distinguish stellar multiplicity between single and multiple planet systems.

### 5.3.3. Stellar multiplicity and close-in planets

Stellar binarity has been hypothesized to be important in shaping the architectures of planetary systems, both by regulating planet formation and by dynamically sculpting planets final orbits, such as forcing Kozai oscillations that cause planet migration (Fabrycky & Tremaine 2007; Katz et al. 2011; Naoz et al. 2012) or by tilting the circumstellar disk (Batygin 2012). If planetary

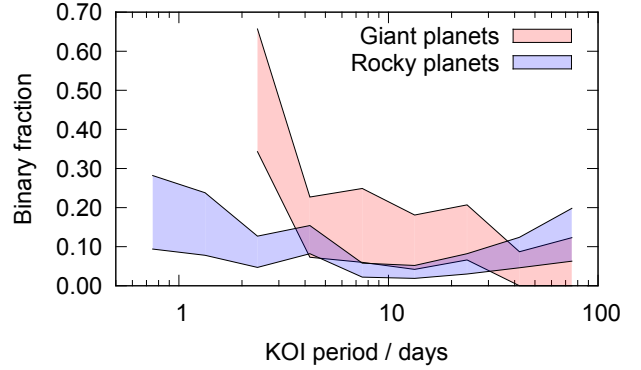


FIG. 11.—  $1\sigma$  uncertainty regions for binarity fraction as a function of KOI period for two different planetary populations (we split “rocky” from “giant” at Neptune’s radius ( $3.8 R_{\oplus}$ ), but the exact value of the split does not significantly affect the uncertainty region shape). The gas giants cut off for shorter periods because of insufficient targets for acceptable statistics

migration is induced by a third body, one would expect to find a correlation between the presence of a detected third body and the presence of short-period planets.

Figure 11 shows the fraction of *Kepler* planet candidates with nearby stars as a function of the period of the closest-in planet, grouping the planets into two different size ranges. From these raw binarity fractions, where we have not accounted for the probability of physical association, it appears that while small planets do not show a significant change in third-body probability with the orbital period of the *Kepler* candidate, giant planets show a significant increase at periods less than  $\sim 15$  days. Binning all our targets into only four population groups allows us to search for smaller changes in the binarity statistics (Figure 12). We see that small planets at short periods share the same binarity fraction as all sizes of planets with  $>15$  days (within statistical errors). However, the short period giant planets again show a significantly increased binarity fraction, at the  $2.1\sigma$  level.

We can attempt to remove the background asterisms by selecting on the basis of contrast ratio, as faint background stars are more likely to be chance alignments than roughly-equal-brightness companions. Our survey displayed an excess of close-separation bright companions: there are 13 companions with  $\Delta M < 2$  with separations  $<1.5''$ , and none at larger radii (Figure 7), while the numbers of fainter companions are less biased. We suggest that this excess reveals a bright-companion population which is more likely to be physically associated than an average companion in the survey.

Selecting the companions with  $\Delta M < 3$  and separation  $<1.5''$  leads an increased difference in stellar multiplicity between the planetary populations, at  $2.6\sigma$  (Figure 13). This approach does not fully account for the probability of each companion being physically associated, and so its results should be interpreted with caution. For example, close-in companions are less likely to be rejected by the *Kepler* centroid-based false-positive tests, but it is not obvious why this rejection would be different for planetary systems with short-period ( $<15$  days) and longer-period KOIs (with a median period of 54d for the KOIs we surveyed). In fact, the shorter-period systems have more eclipse events in the *Kepler* dataset and it should there-

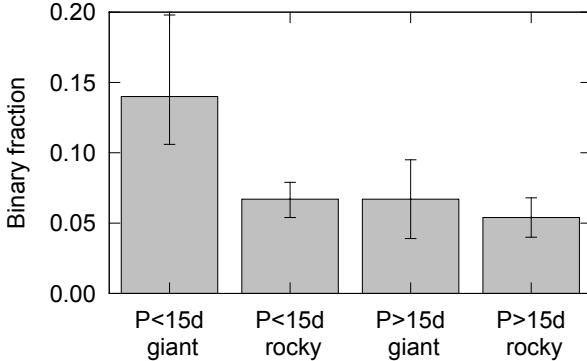


FIG. 12.— Fraction of KOIs with nearby stars for four different planetary populations. Giant here is shorthand for a radius equal to or larger than that of Neptune. We assign KOIs to these populations if any planet in the system meets the requirements; a small number of multiple-planet systems are therefore assigned to multiple populations.

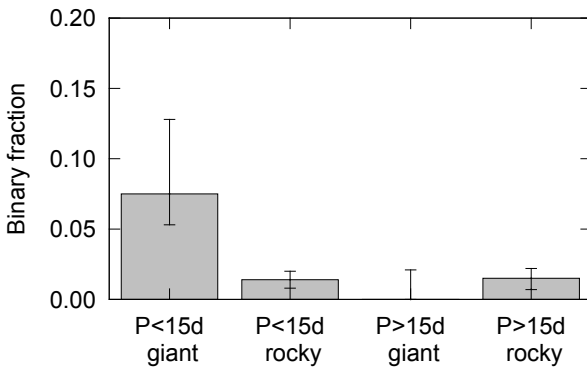


FIG. 13.— Fraction of KOIs with nearby stars for four different planetary populations – as figure 12 with only companions with  $\Delta M < 3$  and separations  $< 1''.5$ , removing faint nearby stars which are less likely to be physically associated (we did not detect any bright companions around the 84 longer-period giant planet KOIs in our survey, so we only show an upper limit). There is a 2.5 $\sigma$ -level detection of a difference in stellar multiplicity rates for close-in giant planets.

fore be easier to detect a small centroid shift from close-in companions.

On the basis of our current analysis, we suggest that the difference of multiplicity rates between the planetary populations may be tentative evidence for third bodies in stellar systems producing an excess of close-in giant planets. We expect the full Robo-AO surveys to be able to evaluate this possibility at more than the 3 $\sigma$  confidence level.

## 6. CONCLUSIONS

We observed 715 *Kepler* planetary system candidates with the Robo-AO robotic laser adaptive optics system. Our detection of 53 planetary candidates with nearby stars from 715 targets implies an overall companion rate of  $7.4\% \pm 1.0\%$  at separations between  $0''.1$  and  $2''.5$ . We have detailed the effects of the detected nearby stars on the interpretation of the *Kepler* planetary candidates, including the detection of probable "co-incident" multiples (KOI-191 and KOI-1151), multiple-planet systems likely containing false positives (KOI-1845), and the confirmation of five KOIs as roughly Earth-radius planets in multiple stellar systems (KOI-1613, KOI-1619, KOI-2059, KOI-2463, and KOI 2657). We have also found tentative, 2.6 $\sigma$ -level, evidence for stellar third bodies leading to a 2-3 $\times$  increased rate of close-in giant planets.

We expect the ongoing Robo-AO surveys to complete observations of every *Kepler* planet candidate by the end of 2014. The increased survey numbers will allow us to search for stellar multiplicity correlations only in multiple-detected-planet systems, which are expected to have a much lower false-positive probability, and thus will improve our ability to disentangle false-positives from astrophysical effects. The number of multiple systems in our current sample is not large enough to verify our tentative conclusions on the effects of stellar multiplicity on short-period giant planets (in particular, we have only covered one multiple-planet system with a short-period giant planet), but we plan to investigate these possibilities in future data releases. We are also continuing observations of our detected companions to search for common-proper-motion pairs. The completed Robo-AO survey will also allow us to confirm many more *Kepler* planet candidates and likely find more exotic planetary systems.

## ACKNOWLEDGEMENTS

The Robo-AO system is supported by collaborating partner institutions, the California Institute of Technology and the Inter-University Centre for Astronomy and Astrophysics, and by the National Science Foundation under Grant Nos. AST-0906060 and AST-0960343, by the Mount Cuba Astronomical Foundation, by a gift from Samuel Oschin. We are grateful to the Palomar Observatory staff for their ongoing support of Robo-AO on the 60-inch telescope, particularly S. Kunsman, M. Doyle, J. Henning, R. Walters, G. Van Idsinga, B. Baker, K. Dunsccombe and D. Roderick. We recognize and acknowledge the very significant cultural role and reverence that the summit of Mauna Kea has always had within the indigenous Hawaiian community. We are most fortunate to have the opportunity to conduct observations from this mountain. J.A.J. acknowledges support from the Alfred P. Sloan Foundation, and the David and Lucile Packard Foundation. *Facilities:* PO:1.5m (Robo-AO), Keck:II (NIRC2)

## REFERENCES

- Adams, E. R., Ciardi, D. R., Dupree, A. K., Gautier, III, T. N., Kulesa, C., & McCarthy, D. 2012, AJ, 144, 42  
 Adams, E. R., Dupree, A. K., Kulesa, C., & McCarthy, D. 2013, AJ, 146, 9  
 Baranec, C., Riddle, R., Law, N. M., Ramaprakash, A., Tendulkar, S. P., Bui, K., Burse, M. P., Chordia, P., Das, H. K., Davis, J. T., Dekany, R. G., Kasliwal, M. M., Kulkarni, S. R., Morton, T. D., Ofek, E. O., & Punnadi, S. 2013, Journal of Visualized Experiments, 72, e50021

- Baranec, C., Riddle, R., Law, N. M., Ramaprakash, A. N., Tendulkar, S. P., Bui, K., Burse, M. P., Chordia, P., Das, H. K., Davis, J. T. C., Dekany, R. G., Kasliwal, M. M., Kulkarni, S. R., Morton, T. D., Ofek, E. O., & Punnadi, S. 2013, ArXiv e-prints
- Baranec, C., Riddle, R., Ramaprakash, A. N., Law, N., Tendulkar, S., Kulkarni, S., Dekany, R., Bui, K., Davis, J., Burse, M., Das, H., Hildebrandt, S., Punnadi, S., & Smith, R. 2012, in , 844704–11
- Baranec, C., Riddle, R., Ramaprakash, A. N., Law, N., Tendulkar, S., Kulkarni, S., Dekany, R., Bui, K., Davis, J., Burse, M., Das, H., Hildebrandt, S., Punnadi, S., & Smith, R. 2012, in Society of Photo-Optical Instrumentation Engineers (SPIE) Conference Series, Vol. 8447, Society of Photo-Optical Instrumentation Engineers (SPIE) Conference Series
- Barclay, T., Rowe, J. F., Lissauer, J. J., Huber, D., Fressin, F., Howell, S. B., Bryson, S. T., Chaplin, W. J., Désert, J.-M., Lopez, E. D., Marcy, G. W., Mullally, F., Ragozzine, D., Torres, G., Adams, E. R., Agol, E., Barrado, D., Basu, S., Bedding, T. R., Buchhave, L. A., Charbonneau, D., Christiansen, J. L., Christensen-Dalsgaard, J., Ciardi, D., Cochran, W. D., Dupree, A. K., Elsworth, Y., Everett, M., Fischer, D. A., Ford, E. B., Fortney, J. J., Geary, J. C., Haas, M. R., Handberg, R., Hekker, S., Henze, C. E., Horch, E., Howard, A. W., Hunter, R. C., Isaacson, H., Jenkins, J. M., Karoff, C., Kawaler, S. D., Kjeldsen, H., Klaus, T. C., Latham, D. W., Li, J., Lillo-Box, J., Lund, M. N., Lundkvist, M., Metcalfe, T. S., Miglio, A., Morris, R. L., Quintana, E. V., Stello, D., Smith, J. C., Still, M., & Thompson, S. E. 2013, Nature, 494, 452
- Barrado, D., Lillo-Box, J., Bouy, H., Aceituno, J., & Sánchez, S. 2013, in European Physical Journal Web of Conferences, Vol. 47, European Physical Journal Web of Conferences, 5008
- Batalha, N. M., Rowe, J. F., Bryson, S. T., Barclay, T., Burke, C. J., Caldwell, D. A., Christiansen, J. L., Mullally, F., Thompson, S. E., Brown, T. M., Dupree, A. K., Fabrycky, D. C., Ford, E. B., Fortney, J. J., Gilliland, R. L., Isaacson, H., Latham, D. W., Marcy, G. W., Quinn, S. N., Ragozzine, D., Shporer, A., Borucki, W. J., Ciardi, D. R., Gautier, III, T. N., Haas, M. R., Jenkins, J. M., Koch, D. G., Lissauer, J. J., Rapin, W., Basri, G. S., Boss, A. P., Buchhave, L. A., Carter, J. A., Charbonneau, D., Christensen-Dalsgaard, J., Clarke, B. D., Cochran, W. D., Demory, B.-O., Desert, J.-M., Devore, E., Doyle, L. R., Esquerdo, G. A., Everett, M., Fressin, F., Geary, J. C., Girouard, F. R., Gould, A., Hall, J. R., Holman, M. J., Howard, A. W., Howell, S. B., Ibrahim, K. A., Kinemuchi, K., Kjeldsen, H., Klaus, T. C., Li, J., Lucas, P. W., Meibom, S., Morris, R. L., Prsa, A., Quintana, E., Sanderfer, D. T., Sasselov, D., Seader, S. E., Smith, J. C., Steffen, J. H., Still, M., Stumpe, M. C., Tarter, J. C., Tenenbaum, P., Torres, G., Twicken, J. D., Uddin, K., Van Cleve, J., Walkowicz, L., & Welsh, W. F. 2013a, ApJS, 204, 24
- . 2013b, ApJS, 204, 24
- Batygin, K. 2012, Nature, 491, 418
- Borucki, W. J., Koch, D., Basri, G., Batalha, N., Brown, T., Caldwell, D., Caldwell, J., Christensen-Dalsgaard, J., Cochran, W. D., DeVore, E., Dunham, E. W., Dupree, A. K., Gautier, T. N., Geary, J. C., Gilliland, R., Gould, A., Howell, S. B., Jenkins, J. M., Kondo, Y., Latham, D. W., Marcy, G. W., Meibom, S., Kjeldsen, H., Lissauer, J. J., Monet, D. G., Morrison, D., Sasselov, D., Tarter, J., Boss, A., Brownlee, D., Owen, T., Buzasi, D., Charbonneau, D., Doyle, L., Fortney, J., Ford, E. B., Holman, M. J., Seager, S., Steffen, J. H., Welsh, W. F., Rowe, J., Anderson, H., Buchhave, L., Ciardi, D., Walkowicz, L., Sherry, W., Horch, E., Isaacson, H., Everett, M. E., Fischer, D., Torres, G., Johnson, J. A., Endl, M., MacQueen, P., Bryson, S. T., Dotson, J., Haas, M., Kolodziejczak, J., Van Cleve, J., Chandrasekaran, H., Twicken, J. D., Quintana, E. V., Clarke, B. D., Allen, C., Li, J., Wu, H., Tenenbaum, P., Verner, E., Bruhwiler, F., Barnes, J., & Prsa, A. 2010, Science, 327, 977
- Borucki, W. J., Koch, D. G., Basri, G., Batalha, N., Brown, T. M., Bryson, S. T., Caldwell, D., Christensen-Dalsgaard, J., Cochran, W. D., DeVore, E., Dunham, E. W., Gautier, III, T. N., Geary, J. C., Gilliland, R., Gould, A., Howell, S. B., Jenkins, J. M., Latham, D. W., Lissauer, J. J., Marcy, G. W., Rowe, J., Sasselov, D., Boss, A., Charbonneau, D., Ciardi, D., Doyle, L., Dupree, A. K., Ford, E. B., Fortney, J., Holman, M. J., Seager, S., Steffen, J. H., Tarter, J., Welsh, W. F., Allen, C., Buchhave, L. A., Christiansen, J. L., Clarke, B. D., Das, S., Désert, J.-M., Endl, M., Fabrycky, D., Fressin, F., Haas, M., Horch, E., Howard, A., Isaacson, H., Kjeldsen, H., Kolodziejczak, J., Kulesa, C., Li, J., Lucas, P. W., Machalek, P., McCarthy, D., MacQueen, P., Meibom, S., Miquel, T., Prsa, A., Quinn, S. N., Quintana, E. V., Ragozzine, D., Sherry, W., Shporer, A., Tenenbaum, P., Torres, G., Twicken, J. D., Van Cleve, J., Walkowicz, L., Witteborn, F. C., & Still, M. 2011, ApJ, 736, 19
- Brown, T. M., Latham, D. W., Everett, M. E., & Esquerdo, G. A. 2011, AJ, 142, 112
- Bryson, S. T., Jenkins, J. M., Gilliland, R. L., Twicken, J. D., Clarke, B., Rowe, J., Caldwell, D., Batalha, N., Mullally, F., Haas, M. R., & Tenenbaum, P. 2013, PASP, 125, 889
- Buchhave, L. A., Latham, D. W., Carter, J. A., Désert, J.-M., Torres, G., Adams, E. R., Bryson, S. T., Charbonneau, D. B., Ciardi, D. R., Kulesa, C., Dupree, A. K., Fischer, D. A., Fressin, F., Gautier, III, T. N., Gilliland, R. L., Howell, S. B., Isaacson, H., Jenkins, J. M., Marcy, G. W., McCarthy, D. W., Rowe, J. F., Batalha, N. M., Borucki, W. J., Brown, T. M., Caldwell, D. A., Christiansen, J. L., Cochran, W. D., Deming, D., Dunham, E. W., Everett, M., Ford, E. B., Fortney, J. J., Geary, J. C., Girouard, F. R., Haas, M. R., Holman, M. J., Horch, E., Klaus, T. C., Knutson, H. A., Koch, D. G., Kolodziejczak, J., Lissauer, J. J., Machalek, P., Mullally, F., Still, M. D., Quinn, S. N., Seager, S., Thompson, S. E., & Van Cleve, J. 2011, ApJS, 197, 3
- Cenko, S. B., Fox, D. B., Moon, D.-S., Harrison, F. A., Kulkarni, S. R., Henning, J. R., Guzman, C. D., Bonati, M., Smith, R. M., Thicksten, R. P., Doyle, M. W., Petrie, H. L., Gal-Yam, A., Soderberg, A. M., Anagnostou, N. L., & Laity, A. C. 2006, The Publications of the Astronomical Society of the Pacific, 118, 1396
- Colón, K. D., Ford, E. B., & Morehead, R. C. 2012, MNRAS, 426, 342
- Dotter, A., Chaboyer, B., Jevremović, D., Kostov, V., Baron, E., & Ferguson, J. W. 2008, ApJS, 178, 89
- Dressing, C. D. & Charbonneau, D. 2013, ApJ, 767, 95
- Fabrycky, D. & Tremaine, S. 2007, ApJ, 669, 1298
- Fressin, F., Torres, G., Charbonneau, D., Bryson, S. T., Christiansen, J., Dressing, C. D., Jenkins, J. M., Walkowicz, L. M., & Batalha, N. M. 2013, ApJ, 766, 81
- Fruchter, A. S. & Hook, R. N. 2002, PASP, 114, 144
- Horch, E. P., Howell, S. B., Everett, M. E., & Ciardi, D. R. 2012, AJ, 144, 165
- Howell, S. B., Everett, M. E., Sherry, W., Horch, E., & Ciardi, D. R. 2011, AJ, 142, 19
- Johnson, J. A., Apps, K., Gazak, J. Z., Crepp, J. R., Crossfield, I. J., Howard, A. W., Marcy, G. W., Morton, T. D., Chubak, C., & Isaacson, H. 2011, ApJ, 730, 79
- Katz, B., Dong, S., & Malhotra, R. 2011, Physical Review Letters, 107, 181101
- Koch, D. G., Borucki, W. J., Basri, G., Batalha, N. M., Brown, T. M., Caldwell, D., Christensen-Dalsgaard, J., Cochran, W. D., DeVore, E., Dunham, E. W., Gautier, III, T. N., Geary, J. C., Gilliland, R. L., Gould, A., Jenkins, J., Kondo, Y., Latham, D. W., Lissauer, J. J., Marcy, G., Monet, D., Sasselov, D., Boss, A., Brownlee, D., Caldwell, J., Dupree, A. K., Howell, S. B., Kjeldsen, H., Meibom, S., Morrison, D., Owen, T., Reitsema, H., Tarter, J., Bryson, S. T., Dotson, J. L., Gazis, P., Haas, M. R., Kolodziejczak, J., Rowe, J. F., Van Cleve, J. E., Allen, C., Chandrasekaran, H., Clarke, B. D., Li, J., Quintana, E. V., Tenenbaum, P., Twicken, J. D., & Wu, H. 2010, ApJ, 713, L79
- Lafrenière, D., Marois, C., Doyon, R., Nadeau, D., & Artigau, É. 2007, ApJ, 660, 770
- Law, N. M., Hodgkin, S. T., & Mackay, C. D. 2006a, MNRAS, 368, 1917

- . 2006b, MNRAS, 368, 1917
- Law, N. M., Kraus, A. L., Street, R., Fulton, B. J., Hillenbrand, L. A., Shporer, A., Lister, T., Baranec, C., Bloom, J. S., Bui, K., Burse, M. P., Cenko, S. B., Das, H. K., Davis, J. T. C., Dekany, R. G., Filippienko, A. V., Kasliwal, M. M., Kulkarni, S. R., Nugent, P., Ofek, E. O., Poznanski, D., Quimby, R. M., Ramaprakash, A. N., Riddle, R., Silverman, J. M., Sivanandam, S., & Tendulkar, S. P. 2012, ApJ, 757, 133
- Law, N. M., Mackay, C. D., Dekany, R. G., Ireland, M., Lloyd, J. P., Moore, A. M., Robertson, J. G., Tuthill, P., & Woodruff, H. C. 2009, ApJ, 692, 924
- Lillo-Box, J., Barrado, D., & Bouy, H. 2012, A&A, 546, A10
- Ming, Y., Hui-Gen, L., Hui, Z., & Ji-Lin, Z. 2013, ArXiv e-prints
- Morton, T. D. 2012, ApJ, 761, 6
- Morton, T. D. & Johnson, J. A. 2011, ApJ, 738, 170
- Naoz, S., Farr, W. M., & Rasio, F. A. 2012, ApJ, 754, L36
- Narita, N., Kudo, T., Bergfors, C., Nagasawa, M., Thalmann, C., Sato, B., Suzuki, R., Kandori, R., Janson, M., Goto, M., Brandner, W., Ida, S., Abe, L., Carson, J., Egner, S. E., Feldt, M., Golota, T., Guyon, O., Hashimoto, J., Hayano, Y., Hayashi, M., Hayashi, S. S., Henning, T., Hodapp, K. W., Ishii, M., Knapp, G. R., Kusakabe, N., Kuzuhara, M., Matsuo, T., McElwain, M. W., Miyama, S. M., Morino, J.-I., Moro-Martín, A., Nishimura, T., Pyo, T.-S., Serabyn, E., Suenaga, T., Suto, H., Takahashi, Y. H., Takami, M., Takato, N., Terada, H., Tomono, D., Turner, E. L., Watanabe, M., Yamada, T., Takami, H., Usuda, T., & Tamura, M. 2010, PASJ, 62, 779
- O'Donovan, F. T., Charbonneau, D., Torres, G., Mandushev, G., Dunham, E. W., Latham, D. W., Alonso, R., Brown, T. M., Esquerdo, G. A., Everett, M. E., & Creevey, O. L. 2006, ApJ, 644, 1237
- Riddle, R. L., Burse, M. P., Law, N. M., Tendulkar, S. P., Baranec, C., Rudy, A. R., Sitt, M., Arya, A., Papadopoulos, A., Ramaprakash, A. N., & Dekany, R. G. 2012, in Society of Photo-Optical Instrumentation Engineers (SPIE) Conference Series, Vol. 8447, Society of Photo-Optical Instrumentation Engineers (SPIE) Conference Series
- Santerne, A., Fressin, F., Díaz, R. F., Figueira, P., Almenara, J.-M., & Santos, N. C. 2013, A&A, 557, A139
- Tenenbaum, P., Jenkins, J. M., Seader, S., Burke, C. J., Christiansen, J. L., Rowe, J. F., Caldwell, D. A., Clarke, B. D., Li, J., Quintana, E. V., Smith, J. C., Thompson, S. E., Twicken, J. D., Borucki, W. J., Batalha, N. M., Cote, M. T., Haas, M. R., Hunter, R. C., Sanderfer, D. T., Girouard, F. R., Hall, J. R., Ibrahim, K., Klaus, T. C., McCauliff, S. D., Middour, C. K., Sabale, A., Uddin, A. K., Wohler, B., Barclay, T., & Still, M. 2013, ApJS, 206, 5
- Terziev, E., Law, N. M., Arcavi, I., Baranec, C., Bloom, J. S., Bui, K., Burse, M. P., Chorida, P., Das, H. K., Dekany, R. G., Kraus, A. L., Kulkarni, S. R., Nugent, P., Ofek, E. O., Punnadi, S., Ramaprakash, A. N., Riddle, R., Sullivan, M., & Tendulkar, S. P. 2013, ApJS, 206, 18
- Wizinowich, P., Acton, D. S., Shelton, C., Stomski, P., Gathright, J., Ho, K., Lupton, W., Tsubota, K., Lai, O., Max, C., Brase, J., An, J., Avicola, K., Olivier, S., Gavel, D., Macintosh, B., Ghez, A., & Larkin, J. 2000, PASP, 112, 315
- York, D. G., Adelman, J., Anderson, Jr., J. E., Anderson, S. F., Annis, J., Bahcall, N. A., Bakken, J. A., Barkhouse, R., Bastian, S., Berman, E., Boroski, W. N., Bracker, S., Briegel, C., Briggs, J. W., Brinkmann, J., Brunner, R., Burles, S., Carey, L., Carr, M. A., Castander, F. J., Chen, B., Colestock, P. L., Connolly, A. J., Crocker, J. H., Csabai, I., Czarapata, P. C., Davis, J. E., Doi, M., Dombeck, T., Eisenstein, D., Ellman, N., Elms, B. R., Evans, M. L., Fan, X., Federwitz, G. R., Fiselli, L., Friedman, S., Frieman, J. A., Fukugita, M., Gillespie, B., Gunn, J. E., Gurbani, V. K., de Haas, E., Haldeman, M., Harris, F. H., Hayes, J., Heckman, T. M., Hennessy, G. S., Hindsley, R. B., Holm, S., Holmgren, D. J., Huang, C.-h., Hull, C., Husby, D., Ichikawa, S.-I., Ichikawa, T., Ivezic, Ž., Kent, S., Kim, R. S. J., Kinney, E., Klaene, M., Kleinman, A. N., Kleinman, S., Knapp, G. R., Korienek, J., Kron, R. G., Kunszt, P. Z., Lamb, D. Q., Lee, B., Leger, R. F., Limmgokol, S., Lindenmeyer, C., Long, D. C., Loomis, C., Loveday, J., Lucinio, R., Lupton, R. H., MacKinnon, B., Mannery, E. J., Mantsch, P. M., Margon, B., McGehee, P., McKay, T. A., Meiksin, A., Merelli, A., Monet, D. G., Munn, J. A., Narayanan, V. K., Nash, T., Neilsen, E., Neswold, R., Newberg, H. J., Nichol, R. C., Nicinski, T., Nonino, M., Okada, N., Okamura, S., Ostriker, J. P., Owen, R., Pauls, A. G., Peoples, J., Peterson, R. L., Petrvick, D., Pier, J. R., Pope, A., Pordes, R., Prosapio, A., Rechenmacher, R., Quinn, T. R., Richards, G. T., Richmond, M. W., Rivetta, C. H., Rockosi, C. M., Ruthmansdorfer, K., Sandford, D., Schlegel, D. J., Schneider, D. P., Sekiguchi, M., Sergey, G., Shimassaku, K., Siegmund, W. A., Smee, S., Smith, J. A., Snedden, S., Stone, R., Stoughton, C., Strauss, M. A., Stubbs, C., SubbaRao, M., Szalay, A. S., Szapudi, I., Szokoly, G. P., Thakar, A. R., Tremonti, C., Tucker, D. L., Uomoto, A., Vanden Berk, D., Vogeley, M. S., Waddell, P., Wang, S.-i., Watanabe, M., Weinberg, D. H., Yanny, B., Yasuda, N., & SDSS Collaboration. 2000, AJ, 120, 1579

## APPENDIX

TABLE 5  
FULL ROBO-AO OBSERVATION LIST

KOI	$m_i$ / mags	Obs. date	Filter	Obs. qual.	Companion?
K00001.01	11.168	2012/07/16	i	high	yes
K00002.01		2012/07/16	i	high	
K00003.01		2012/07/16	i	high	
K00005.01	11.485	2012/07/16	i	high	
K00007.01	12.038	2012/07/16	i	high	
K00010.01	13.424	2012/07/16	i	medium	
K00012.01	11.245	2012/07/17	i	high	
K00013.01	10.548	2012/10/06	i	high	yes
K00017.01	13.094	2012/07/16	i	medium	
K00018.01	13.148	2012/07/16	i	medium	
K00022.01	13.265	2012/07/16	i	medium	
K00041.01	11.03	2012/07/16	i	high	
K00044.01	13.268	2012/07/16	i	low	
K00046.01	13.497	2012/07/16	i	medium	

TABLE 5 — *Continued*

KOI	$m_i$ / mags	Obs. date	Filter	Obs. qual.	Companion?
K00049.01	13.508	2012/07/16	i	low	
K00063.01	11.379	2012/07/16	i	high	
K00064.01	12.866	2012/07/16	i	medium	
K00069.01	9.739	2012/07/16	i	high	
K00070.01	12.284	2012/07/16	i	medium	
K00075.01	10.617	2012/07/16	i	high	
K00082.01	11.15	2012/07/16	i	high	
K00084.01	11.694	2012/07/16	i	high	
K00085.01	10.882	2012/07/16	i	high	
K00087.01	11.478	2012/07/16	i	high	
K00089.01	11.649	2012/07/16	i	medium	
K00092.01	11.506	2012/07/16	i	high	
K00094.01	12.057	2012/07/16	i	medium	
K00097.01	12.724	2012/07/17	i	medium	yes
K00098.01	12.024	2012/07/17	i	high	yes
K00099.01	12.68	2012/07/16	i	medium	
K00100.01	12.466	2012/07/16	i	medium	
K00102.01	12.384	2012/07/16	i	medium	
K00103.01	12.399	2012/07/16	i	medium	
K00105.01	12.649	2012/07/16	i	medium	
K00107.01	12.53	2012/07/16	i	medium	
K00108.01	12.132	2012/07/16	i	high	
K00110.01	12.545	2012/07/16	i	medium	
K00111.01	12.442	2012/07/16	i	medium	
K00112.01	12.602	2012/07/18	i	medium	
K00113.01	12.163	2012/07/17	i	high	
K00115.01	12.654	2012/07/16	i	medium	
K00117.01	12.309	2012/07/16	i	medium	
K00118.01	12.195	2012/07/17	i	medium	
K00119.01	12.452	2012/07/16	i	low	yes
K00122.01	12.161	2012/07/16	i	medium	
K00124.01	12.784	2012/07/16	i	low	
K00128.01	13.54	2012/07/16	i	low	
K00131.01	13.64	2012/07/16	i	low	
K00137.01	13.287	2012/07/17	i	low	
K00139.01	13.327	2012/07/17	i	low	
K00141.01	13.441	2012/07/18	i	medium	yes
K00142.01	12.895	2012/07/17	i	low	
K00144.01	13.329	2012/07/17	i	low	
K00148.01	12.761	2012/07/17	i	low	
K00149.01	13.167	2012/07/17	i	low	
K00152.01	13.761	2012/07/17	i	low	
K00153.01	13.097	2012/07/17	LP600	medium	
K00156.01	13.334	2012/09/01	LP600	high	
K00157.01	13.508	2012/09/01	LP600	high	
K00159.01	13.243	2012/07/18	LP600	high	
K00161.01	12.99	2012/07/18	LP600	high	
K00162.01	13.626	2012/07/18	LP600	medium	yes
K00165.01	13.665	2012/07/17	LP600	medium	
K00166.01	13.315	2012/07/17	LP600	medium	
K00167.01	13.15	2012/07/17	LP600	high	
K00168.01	13.244	2012/07/17	LP600	high	
K00171.01	13.575	2012/07/17	LP600	high	
K00172.01	13.559	2012/07/18	LP600	high	
K00173.01	13.659	2012/07/18	LP600	high	
K00174.01	13.449	2012/07/18	LP600	high	yes
K00176.01	13.307	2012/07/18	LP600	high	
K00177.01	12.979	2012/07/18	i	medium	yes
K00179.01	13.765	2012/07/18	LP600	high	
K00180.01	12.813	2012/07/18	i	medium	
K00191.01	14.747	2012/09/01	LP600	low	yes
K00197.01	13.706	2012/07/18	i	medium	
K00201.01	13.785	2012/07/18	LP600	high	
K00203.01	13.928	2012/07/18	LP600	high	
K00209.01	14.131	2012/09/01	LP600	medium	
K00211.01	14.82	2012/09/14	LP600	low	
K00214.01	14.003	2012/07/18	LP600	high	
K00216.01	14.4	2012/09/01	LP600	low	
K00219.01	13.925	2012/07/18	LP600	high	
K00220.01	14.011	2012/09/01	LP600	medium	
K00222.01	14.315	2012/09/01	LP600	low	
K00223.01	14.447	2012/09/01	LP600	medium	
K00232.01	14.067	2012/07/18	LP600	medium	
K00237.01	13.964	2012/07/18	LP600	medium	

TABLE 5 — *Continued*

KOI	m <sub>i</sub> / mags	Obs. date	Filter	Obs. qual.	Companion?
K00238.01	13.891	2012/09/01	LP600	medium	
K00241.01	13.881	2012/07/18	LP600	medium	
K00244.01		2012/07/18	i	high	
K00246.01	9.82	2012/07/18	i	high	
K00247.01	13.585	2012/08/03	LP600	high	
K00248.01	14.68	2012/08/03	LP600	medium	
K00250.01	14.887	2012/08/03	LP600	low	
K00253.01	14.667	2012/08/03	LP600	medium	
K00254.01	15.364	2012/08/03	LP600	low	
K00256.01	14.636	2012/07/15	LP600	medium	
K00260.01		2012/07/18	i	high	
K00261.01	10.109	2012/07/18	i	high	
K00263.01	10.647	2012/07/18	i	high	
K00268.01		2012/09/14	LP600	high	yes
K00269.01	10.823	2012/07/18	i	high	
K00270.01		2012/07/17	i	high	
K00273.01	11.262	2012/07/18	i	high	
K00275.01		2012/07/18	i	high	
K00276.01	11.711	2012/07/18	i	high	
K00277.01		2012/07/18	i	high	
K00279.01	11.563	2012/07/18	i	medium	
K00281.01	11.77	2012/07/18	i	high	
K00282.01		2012/07/18	i	high	
K00283.01	11.334	2012/07/18	i	high	
K00288.01		2012/07/18	i	high	
K00291.01	12.642	2012/07/18	i	high	
K00294.01	12.511	2012/07/18	i	high	
K00296.01	12.77	2012/08/02	i	medium	
K00297.01	12.042	2012/08/02	i	high	
K00299.01	12.675	2012/07/18	i	medium	
K00301.01	12.586	2012/07/18	i	high	
K00302.01	11.969	2012/07/18	i	high	
K00303.01	11.994	2012/07/18	i	high	
K00305.01	12.606	2012/07/18	i	medium	
K00306.01	12.363	2012/07/18	i	low	yes
K00307.01	12.65	2012/08/02	i	medium	
K00308.01	12.205	2012/07/18	i	medium	
K00312.01		2012/07/28	i	high	
K00313.01	12.736	2012/08/02	i	high	
K00314.01	12.457	2012/08/03	LP600	high	
K00315.01	12.63	2012/07/28	i	medium	
K00316.01	12.494	2012/08/02	i	high	
K00317.01	12.751	2012/07/28	i	medium	
K00319.01		2012/08/02	i	high	
K00321.01	12.312	2012/08/02	i	high	
K00323.01	12.24	2012/08/02	i	high	
K00327.01	12.858	2012/08/02	i	medium	
K00330.01	13.73	2012/07/28	LP600	high	
K00331.01	13.277	2012/07/28	i	medium	
K00332.01	12.847	2012/07/28	i	high	
K00333.01	13.265	2012/08/02	i	medium	
K00337.01	13.746	2012/08/02	LP600	medium	
K00339.01	13.616	2012/08/02	LP600	medium	
K00340.01	12.82	2012/07/28	i	medium	
K00341.01	13.106	2012/07/28	i	medium	
K00343.01	13.013	2012/08/02	i	medium	
K00344.01	13.211	2012/08/02	i	medium	
K00345.01	13.005	2012/08/02	i	medium	
K00348.01	13.555	2012/08/03	LP600	high	
K00349.01	13.382	2012/08/02	LP600	high	
K00350.01	13.202	2012/08/02	i	medium	
K00352.01	13.579	2012/07/28	LP600	high	
K00353.01	13.251	2012/08/02	i	low	
K00356.01	13.532	2012/07/28	LP600	high	yes
K00360.01	12.823	2012/08/02	i	medium	
K00361.01	12.914	2012/08/02	i	medium	
K00365.01	10.992	2012/07/28	i	high	
K00366.01		2012/08/02	i	high	
K00368.01	11.598	2012/08/02	i	high	
K00371.01	11.895	2012/07/28	i	high	
K00372.01	12.208	2012/07/28	i	high	
K00373.01	12.593	2012/08/02	i	medium	
K00377.01	13.613	2012/09/01	LP600	medium	
K00384.01	13.106	2012/08/02	i	low	

TABLE 5 — *Continued*

KOI	$m_i$ / mags	Obs. date	Filter	Obs. qual.	Companion?
K00385.01	13.211	2012/08/02	i	medium	
K00386.01	13.661	2012/08/02	i	low	
K00388.01	13.448	2012/08/02	i	medium	
K00392.01	13.745	2012/08/05	LP600	medium	
K00393.01	13.395	2012/08/02	i	low	
K00401.01	13.729	2012/08/05	LP600	medium	yes
K00403.01	13.953	2012/08/05	LP600	medium	
K00408.01	14.766	2012/09/01	LP600	low	
K00409.01	13.965	2012/09/14	LP600	medium	
K00413.01	14.512	2012/09/01	LP600	low	
K00415.01	13.914	2012/08/05	LP600	medium	
K00416.01	14.019	2012/09/01	LP600	low	
K00427.01	14.37	2012/09/01	LP600	low	
K00431.01	14.004	2012/09/01	LP600	medium	
K00435.01	14.342	2012/09/01	LP600	low	
K00439.01	14.063	2012/08/05	LP600	medium	
K00440.01	13.861	2012/09/01	LP600	medium	
K00442.01	13.806	2012/08/05	LP600	medium	
K00444.01	13.909	2012/08/05	LP600	medium	
K00456.01	14.407	2012/09/01	LP600	medium	
K00457.01	13.894	2012/09/01	LP600	medium	
K00459.01	14.028	2012/09/01	LP600	medium	
K00463.01	13.999	2012/08/03	LP600	medium	
K00464.01	14.113	2012/09/01	LP600	medium	
K00465.01	14.017	2012/08/05	LP600	medium	
K00471.01	14.198	2012/09/01	LP600	medium	
K00474.01	14.131	2012/09/01	LP600	low	
K00478.01	13.58	2012/08/04	LP600	high	
K00481.01	14.446	2012/09/01	LP600	medium	
K00486.01	13.934	2012/08/05	LP600	medium	
K00490.01	13.688	2012/08/05	LP600	medium	
K00497.01	14.423	2012/09/01	LP600	low	
K00508.01	14.146	2012/09/01	LP600	medium	
K00509.01	14.638	2012/09/01	LP600	low	
K00511.01	14.017	2012/09/01	LP600	medium	yes
K00517.01	13.806	2012/08/05	LP600	high	
K00519.01	14.737	2012/09/01	LP600	medium	
K00520.01	14.255	2012/09/01	LP600	medium	
K00523.01	14.822	2012/09/01	LP600	low	
K00528.01	14.364	2012/09/01	LP600	low	
K00531.01	13.849	2012/08/03	LP600	high	
K00534.01	14.344	2012/09/01	LP600	medium	
K00542.01	14.12	2012/09/01	LP600	medium	
K00543.01	14.442	2012/09/01	LP600	low	
K00546.01	14.717	2012/09/01	LP600	low	
K00548.01	13.874	2012/08/05	LP600	medium	
K00550.01	13.869	2012/08/05	LP600	medium	
K00551.01	14.725	2012/09/01	LP600	low	
K00555.01	14.499	2012/08/05	LP600	medium	
K00561.01	13.732	2012/08/05	LP600	medium	
K00564.01	14.642	2012/09/02	LP600	low	
K00567.01	14.126	2012/09/02	LP600	medium	
K00568.01	13.895	2012/08/05	LP600	medium	
K00569.01	14.172	2012/09/02	LP600	medium	
K00571.01	14.015	2012/08/03	LP600	high	
K00572.01	13.96	2012/07/28	i	low	
K00574.01	14.579	2012/09/02	LP600	low	
K00579.01	13.858	2012/08/05	LP600	medium	
K00582.01	14.529	2012/09/02	LP600	medium	
K00590.01	14.444	2012/09/02	LP600	low	
K00593.01	14.754	2012/09/02	LP600	low	
K00597.01	14.721	2012/09/02	LP600	low	
K00601.01	14.515	2012/09/02	LP600	medium	
K00611.01	13.866	2012/08/05	LP600	medium	
K00612.01	13.871	2012/08/05	LP600	medium	
K00620.01	14.467	2012/09/02	LP600	medium	
K00623.01	11.685	2012/08/03	i	high	
K00624.01	13.39	2012/08/03	i	medium	
K00625.01	13.433	2012/08/03	i	medium	
K00626.01	13.339	2012/08/03	i	medium	
K00627.01	13.119	2012/08/03	i	medium	
K00628.01	13.744	2012/08/03	i	medium	yes
K00629.01	13.788	2012/08/04	i	medium	
K00632.01	13.124	2012/08/04	i	medium	

TABLE 5 — *Continued*

KOI	m <sub>i</sub> / mags	Obs. date	Filter	Obs. qual.	Companion?
K00633.01	13.663	2012/08/04	i	medium	
K00635.01	12.88	2012/08/04	i	medium	
K00638.01	13.394	2012/08/04	i	medium	
K00639.01	13.354	2012/07/28	i	medium	
K00640.01	13.058	2012/07/28	i	low	yes
K00644.01	13.474	2012/08/04	i	medium	
K00647.01	13.413	2012/08/04	i	medium	
K00649.01	13.157	2012/08/04	i	medium	
K00650.01	13.293	2012/08/04	i	medium	
K00654.01	13.789	2012/08/04	i	medium	
K00655.01	12.872	2012/08/04	i	medium	
K00657.01	13.517	2012/08/04	i	medium	
K00658.01	13.789	2012/08/04	i	medium	
K00659.01	13.297	2012/08/04	i	medium	
K00660.01	13.283	2012/08/04	i	medium	
K00661.01	13.731	2012/08/04	i	medium	
K00662.01	13.168	2012/08/04	i	medium	
K00663.01	13.016	2012/09/02	LP600	high	
K00664.01	13.287	2012/08/04	i	medium	
K00665.01	13.005	2012/08/04	i	medium	
K00666.01	13.518	2012/08/04	i	medium	
K00671.01	13.511	2012/08/04	i	medium	
K00673.01	13.211	2012/08/04	i	medium	
K00674.01	13.435	2012/08/04	i	medium	
K00676.01	13.371	2012/09/02	LP600	high	
K00679.01	13.038	2012/08/04	i	medium	
K00680.01	13.485	2012/08/04	i	medium	
K00682.01	13.692	2012/08/04	i	medium	
K00684.01	13.575	2012/08/04	i	medium	
K00685.01	13.77	2012/08/04	i	medium	
K00686.01	13.346	2012/08/04	i	medium	
K00687.01	13.613	2012/08/04	i	medium	
K00688.01	13.849	2012/09/14	LP600	medium	yes
K00689.01	13.548	2012/08/04	i	medium	yes
K00691.01	13.803	2012/08/05	i	low	
K00692.01	13.457	2012/08/05	i	medium	
K00694.01	13.741	2012/08/05	i	low	
K00695.01	13.276	2012/08/05	i	medium	
K00698.01	13.52	2012/08/05	i	low	
K00700.01	13.38	2012/08/05	i	medium	
K00701.01	13.429	2012/08/05	i	low	
K00703.01	13.162	2012/08/05	i	medium	
K00704.01	13.46	2012/08/05	i	medium	
K00707.01	13.815	2012/08/05	i	low	
K00708.01	13.837	2012/08/05	i	low	
K00709.01	13.716	2012/08/05	i	medium	
K00710.01	13.128	2012/08/05	i	medium	
K00711.01	13.735	2012/08/05	i	medium	
K00712.01	13.51	2012/08/05	i	medium	yes
K00714.01	13.184	2012/08/05	i	medium	
K00716.01	13.576	2012/08/05	i	low	
K00717.01	13.182	2012/08/05	i	medium	
K00718.01	13.588	2012/08/05	i	low	
K00719.01	12.899	2012/08/05	i	medium	
K00720.01	13.489	2012/08/05	i	low	
K00721.01	13.439	2012/08/05	i	low	
K00722.01	13.343	2012/08/05	i	high	
K00723.01	14.795	2012/09/02	LP600	low	
K00738.01	15.063	2012/09/02	LP600	low	
K00739.01	14.931	2012/08/03	LP600	medium	
K00756.01	15.492	2012/09/02	LP600	low	
K00781.01	15.267	2012/08/03	LP600	low	
K00800.01	15.341	2012/09/02	LP600	low	
K00817.01	14.793	2012/08/03	LP600	medium	
K00818.01	15.192	2012/08/04	LP600	medium	
K00834.01	14.862	2012/09/02	LP600	low	
K00835.01	14.884	2012/09/02	LP600	low	
K00837.01	15.325	2012/09/02	LP600	low	
K00842.01	15.001	2012/09/02	LP600	low	
K00853.01	15.039	2012/09/02	LP600	low	
K00854.01	15.162	2012/08/03	LP600	low	
K00857.01	14.787	2012/09/02	LP600	low	
K00872.01	14.98	2012/09/02	LP600	low	
K00874.01	14.716	2012/09/02	LP600	low	

TABLE 5 — *Continued*

KOI	$m_i$ / mags	Obs. date	Filter	Obs. qual.	Companion?
K00877.01	14.547	2012/06/17	LP600	low	
K00880.01	14.918	2012/09/02	LP600	low	
K00884.01	14.755	2012/09/02	LP600	low	
K00886.01	15.175	2012/08/04	LP600	medium	
K00896.01	14.974	2012/09/02	LP600	low	
K00898.01	15.221	2012/08/04	LP600	medium	
K00899.01	14.543	2012/08/04	LP600	medium	
K00906.01	15.155	2012/09/02	LP600	low	
K00907.01	14.983	2012/09/02	LP600	low	
K00921.01	15.229	2012/09/02	LP600	low	
K00935.01	15.086	2012/09/02	LP600	low	
K00936.01	14.371	2012/08/04	LP600	medium	
K00938.01	15.328	2012/09/02	LP600	low	
K00939.01	14.849	2012/09/02	LP600	low	
K00947.01	14.564	2012/08/04	LP600	medium	
K00975.01		2012/07/17	i	high	
K00977.01		2012/08/03	i	high	
K00984.01	11.353	2012/08/03	i	high	yes
K00986.01	13.908	2012/08/03	i	low	
K00987.01	12.327	2012/08/03	i	medium	yes
K00988.01	13.259	2012/08/03	i	medium	
K00991.01	13.368	2012/08/03	i	medium	
K01001.01	12.851	2012/08/03	i	medium	
K01002.01	13.362	2012/08/03	i	medium	yes
K01010.01	13.463	2012/08/03	i	medium	
K01015.01	14.349	2012/09/03	LP600	medium	
K01019.01	9.961	2012/08/03	i	high	
K01020.01	12.712	2012/08/03	i	medium	
K01032.01	13.497	2012/08/03	i	medium	
K01050.01	13.696	2012/08/03	i	low	yes
K01052.01	15.201	2012/09/03	LP600	medium	
K01054.01	11.662	2012/08/03	i	high	
K01060.01	14.221	2012/09/03	LP600	medium	
K01070.01	15.348	2012/09/03	LP600	low	
K01078.01	14.846	2012/08/04	LP600	medium	
K01085.01	14.651	2012/08/04	LP600	medium	
K01089.01	14.501	2012/09/03	LP600	medium	
K01102.01	14.711	2012/08/05	LP600	low	
K01113.01	13.54	2012/08/05	i	medium	
K01115.01	13.739	2012/08/05	i	low	
K01116.01	13.153	2012/08/05	i	medium	
K01118.01	13.672	2012/08/05	i	medium	
K01127.01	15.587	2012/09/03	LP600	low	
K01128.01	13.277	2012/08/05	i	medium	
K01141.01	15.39	2012/08/04	LP600	low	
K01145.01	13.956	2012/08/05	i	low	
K01146.01	15.043	2012/07/15	LP600	low	
K01148.01	13.769	2012/08/05	i	medium	
K01150.01	13.139	2012/08/05	i	medium	yes
K01151.01	13.198	2012/08/05	i	medium	yes
K01152.01	13.622	2012/09/14	LP600	low	yes
K01161.01	14.391	2012/09/03	LP600	medium	
K01162.01	12.622	2012/08/04	i	high	
K01163.01	14.735	2012/09/03	LP600	medium	
K01165.01	13.699	2012/08/05	i	medium	
K01168.01	13.851	2012/08/05	i	low	
K01169.01	13.071	2012/08/05	i	medium	
K01175.01	13.075	2012/08/05	i	medium	
K01194.01	15.391	2012/09/03	LP600	medium	
K01198.01	15.165	2012/09/03	LP600	low	
K01202.01	15.352	2012/08/04	LP600	low	
K01203.01	15.159	2012/09/03	LP600	low	
K01208.01	13.456	2012/08/06	i	medium	
K01215.01	13.226	2012/08/06	i	medium	
K01216.01	13.28	2012/08/05	i	low	
K01218.01	13.13	2012/08/06	i	medium	
K01220.01	12.713	2012/08/06	i	medium	
K01221.01	11.265	2012/08/06	i	high	
K01222.01	11.909	2012/08/06	i	high	
K01227.01	13.785	2012/09/14	LP600	low	
K01230.01	11.914	2012/08/06	i	high	
K01236.01	13.518	2012/08/06	i	low	
K01239.01	14.812	2012/09/03	LP600	medium	
K01240.01	14.242	2012/09/03	LP600	medium	

TABLE 5 — *Continued*

KOI	m <sub>i</sub> / mags	Obs. date	Filter	Obs. qual.	Companion?
K01241.01	12.09	2012/09/14	LP600	high	
K01242.01	13.611	2012/08/06	i	low	
K01257.01	14.367	2012/09/14	LP600	low	
K01258.01	15.528	2012/09/03	LP600	medium	
K01266.01	14.869	2012/06/17	LP600	low	
K01270.01	14.544	2012/09/03	LP600	medium	
K01271.01	13.5	2012/08/06	i	low	
K01274.01	13.107	2012/08/06	i	medium	yes
K01275.01	13.442	2012/07/28	i	low	
K01276.01	14.542	2012/09/03	LP600	medium	
K01278.01	15.02	2012/09/03	LP600	medium	
K01279.01	13.555	2012/08/06	i	low	
K01282.01	12.399	2012/08/06	i	high	
K01283.01		2012/08/06	i	high	
K01288.01	14.967	2012/09/14	LP600	low	
K01299.01	11.878	2012/08/06	i	high	
K01301.01	15.581	2012/09/03	LP600	low	
K01305.01	14.913	2012/09/03	LP600	medium	
K01306.01	15.374	2012/09/04	LP600	low	
K01307.01	14.551	2012/09/04	LP600	medium	
K01308.01	13.781	2012/08/06	i	low	
K01309.01	13.727	2012/08/06	i	medium	
K01314.01	12.941	2012/08/06	i	medium	
K01315.01	12.998	2012/08/06	i	medium	
K01316.01	11.694	2012/08/06	i	high	
K01322.01	14.919	2012/09/03	LP600	medium	
K01335.01	13.774	2012/08/06	i	low	
K01336.01	14.61	2012/09/04	LP600	medium	
K01338.01	14.385	2012/09/04	LP600	medium	
K01342.01	14.033	2012/09/04	LP600	medium	
K01344.01	13.269	2012/08/06	i	medium	
K01353.01	13.764	2012/08/06	i	medium	
K01358.01	15.117	2012/09/04	LP600	low	
K01359.01	15.025	2012/09/04	LP600	medium	yes
K01360.01	15.293	2012/09/04	LP600	low	
K01363.01	15.719	2012/09/04	LP600	low	
K01364.01	15.669	2012/09/04	LP600	low	
K01366.01	15.138	2012/09/04	LP600	medium	
K01375.01	13.533	2012/08/06	i	medium	yes
K01376.01	13.902	2012/08/06	i	medium	
K01378.01	13.327	2012/08/06	i	medium	
K01379.01	13.499	2012/08/06	i	medium	
K01393.01	15.201	2012/07/15	LP600	low	
K01396.01	15.62	2012/09/04	LP600	medium	
K01401.01	13.316	2012/08/06	i	medium	
K01408.01	14.141	2012/08/04	LP600	medium	
K01412.01	13.434	2012/08/06	i	medium	
K01422.01	15.194	2012/08/04	LP600	low	
K01426.01	14.063	2012/08/06	i	medium	
K01427.01	15.287	2012/08/04	LP600	medium	
K01435.01	14.012	2012/09/04	LP600	medium	
K01436.01	14.061	2012/09/04	LP600	medium	
K01438.01	13.858	2012/08/06	i	medium	
K01439.01	12.689	2012/08/06	i	medium	
K01442.01	12.296	2012/08/06	i	high	yes
K01444.01	13.784	2012/08/06	i	low	
K01452.01	13.525	2012/08/06	i	medium	
K01459.01	15.139	2012/08/04	LP600	medium	
K01478.01	12.254	2012/08/06	i	high	
K01480.01	15.573	2012/09/04	LP600	low	
K01486.01	15.286	2012/09/04	LP600	medium	
K01515.01	13.862	2012/09/04	LP600	medium	
K01525.01	12.009	2012/08/06	i	high	
K01528.01	13.822	2012/08/06	i	medium	
K01529.01	14.152	2012/09/04	LP600	high	
K01530.01	12.88	2012/08/06	i	medium	
K01535.01	12.884	2012/08/06	i	medium	
K01536.01	12.542	2012/08/06	i	medium	
K01537.01		2012/08/29	i	high	
K01557.01	14.457	2012/09/04	LP600	medium	
K01563.01	15.475	2012/09/04	LP600	low	
K01567.01	15.254	2012/09/04	LP600	medium	
K01576.01	13.826	2012/08/06	i	medium	
K01588.01	14.184	2012/06/17	LP600	medium	

TABLE 5 — *Continued*

KOI	$m_i$ / mags	Obs. date	Filter	Obs. qual.	Companion?
K01589.01	14.547	2012/09/04	LP600	medium	
K01590.01	15.326	2012/09/04	LP600	low	
K01596.01	14.758	2012/06/17	LP600	low	
K01597.01	12.598	2012/08/06	i	high	
K01598.01	14.063	2012/09/04	LP600	medium	
K01606.01	13.752	2012/08/06	i	medium	
K01608.01	13.647	2012/09/04	LP600	high	
K01609.01	13.793	2012/08/29	i	low	
K01612.01	8.658	2012/08/06	i	high	
K01613.01		2012/08/29	i	high	yes
K01615.01	11.341	2012/08/29	i	high	
K01616.01	11.396	2012/08/29	i	high	
K01618.01	11.473	2012/08/29	i	high	
K01619.01	11.427	2012/08/29	i	high	yes
K01621.01	11.711	2012/08/29	i	high	
K01622.01	12.033	2012/08/29	i	high	
K01627.01	15.493	2012/09/04	LP600	low	
K01628.01	12.775	2012/08/29	i	medium	
K01629.01	13.381	2012/08/29	i	medium	
K01632.01	13.157	2012/08/29	i	medium	
K01647.01	13.961	2012/09/04	LP600	high	
K01649.01	14.347	2012/07/16	LP600	medium	
K01655.01	13.559	2012/09/14	LP600	medium	
K01665.01	13.871	2012/09/04	LP600	high	
K01669.01	14.018	2012/09/14	LP600	low	
K01677.01	14.073	2012/09/04	LP600	medium	yes
K01684.01	12.717	2012/09/14	LP600	high	
K01692.01	12.313	2012/09/04	LP600	high	
K01701.01	11.047	2012/08/04	i	high	
K01706.01	13.835	2012/09/14	LP600	medium	
K01713.01	14.712	2012/09/13	LP600	medium	
K01715.01	12.751	2012/08/29	i	medium	
K01725.01	13.107	2012/08/29	i	medium	
K01726.01	12.684	2012/08/29	i	medium	
K01738.01	13.032	2012/08/29	i	medium	
K01751.01	14.248	2012/09/13	LP600	medium	
K01754.01	13.775	2012/09/14	LP600	medium	
K01779.01	13.077	2012/08/29	i	low	
K01781.01	11.884	2012/09/13	LP600	high	
K01783.01	13.774	2012/09/14	LP600	medium	
K01802.01	13.175	2012/08/29	i	medium	
K01803.01	12.932	2012/08/29	i	medium	
K01805.01	13.591	2012/09/14	LP600	medium	
K01812.01	13.582	2012/08/29	i	medium	
K01813.01	13.525	2012/08/29	i	medium	
K01814.01	12.453	2012/09/14	LP600	high	
K01818.01	13.881	2012/09/14	LP600	medium	
K01819.01	13.347	2012/08/29	i	medium	
K01820.01	13.292	2012/09/13	LP600	high	
K01822.01	12.281	2012/08/29	i	medium	
K01824.01	12.567	2012/08/29	i	medium	
K01825.01	13.632	2012/09/14	LP600	high	
K01831.01	13.866	2012/09/14	LP600	medium	
K01832.01	14.776	2012/09/13	LP600	low	
K01835.01	13.388	2012/09/13	LP600	high	
K01839.01	12.992	2012/08/29	i	medium	
K01843.01	13.708	2012/08/29	i	medium	
K01845.01	14.05	2012/09/13	LP600	medium	yes
K01850.01	13.952	2012/09/14	LP600	medium	
K01852.01	12.97	2012/08/29	i	medium	
K01854.01	13.293	2012/08/29	i	medium	
K01856.01	13.804	2012/09/14	LP600	medium	
K01857.01	13.548	2012/08/29	i	medium	
K01860.01	13.822	2012/09/14	LP600	medium	
K01862.01	13.453	2012/08/29	i	medium	
K01863.01	13.473	2012/08/29	i	low	
K01867.01	14.404	2012/07/15	LP600	low	
K01868.01	14.652	2012/07/15	LP600	low	
K01874.01	14.947	2012/09/13	LP600	low	
K01878.01	12.835	2012/08/29	i	medium	
K01880.01	13.835	2012/07/15	LP600	medium	yes
K01883.01	11.757	2012/08/29	i	high	
K01884.01	15.158	2012/09/13	LP600	low	yes
K01886.01	12.087	2012/08/29	i	high	

TABLE 5 — *Continued*

KOI	m <sub>i</sub> / mags	Obs. date	Filter	Obs. qual.	Companion?
K01888.01	13.15	2012/08/29	i	medium	
K01889.01	15.109	2012/09/13	LP600	medium	
K01890.01	11.555	2012/08/29	i	high	yes
K01891.01	14.957	2012/09/13	LP600	medium	yes
K01893.01	13.876	2012/09/14	LP600	medium	
K01894.01	13.05	2012/09/14	LP600	high	
K01895.01	15.42	2012/09/13	LP600	low	
K01897.01	13.779	2012/09/14	LP600	high	
K01905.01	13.713	2012/09/14	LP600	medium	
K01907.01	14.699	2012/07/15	LP600	low	
K01909.01	12.612	2012/09/13	LP600	high	
K01913.01	13.083	2012/08/29	i	medium	
K01915.01	13.809	2012/09/14	LP600	medium	
K01916.01	13.42	2012/09/13	LP600	high	yes
K01917.01	13.479	2012/08/29	i	medium	
K01921.01	12.708	2012/09/14	LP600	high	
K01922.01	15.159	2012/09/13	LP600	medium	
K01923.01	13.879	2012/08/29	i	low	
K01924.01	7.674	2012/08/29	i	high	
K01925.01	9.211	2012/08/29	i	high	
K01929.01	12.53	2012/09/13	LP600	high	
K01930.01	11.957	2012/09/13	LP600	high	
K01931.01	14.307	2012/09/13	LP600	medium	
K01932.01	12.366	2012/09/14	LP600	high	
K01938.01	13.766	2012/09/14	LP600	medium	
K01940.01	14.912	2012/09/13	LP600	medium	
K01944.01	13.79	2012/09/14	LP600	medium	
K01945.01	14.267	2012/09/13	LP600	medium	
K01952.01	14.398	2012/09/13	LP600	medium	
K01955.01	13.025	2012/09/13	LP600	high	
K01960.01	13.975	2012/09/14	LP600	low	
K01961.01	12.61	2012/08/30	i	medium	
K01962.01		2012/08/30	i	high	
K01964.01	10.464	2012/08/30	i	high	
K01970.01	15.141	2012/09/13	LP600	low	
K01977.01	13.566	2012/10/06	LP600	high	
K01979.01	12.786	2012/08/30	i	medium	yes
K01984.01	13.528	2012/08/30	i	medium	
K01988.01	13.741	2012/09/14	LP600	medium	
K02001.01	12.82	2012/08/30	i	medium	
K02002.01	13.104	2012/08/30	i	medium	
K02004.01	13.15	2012/08/30	i	medium	
K02006.01	13.626	2012/07/16	LP600	high	
K02009.01	13.616	2012/09/14	LP600	medium	yes
K02010.01	13.054	2012/08/30	i	medium	
K02011.01	12.419	2012/09/14	LP600	high	
K02013.01	12.665	2012/08/30	i	medium	
K02016.01	13.954	2012/09/14	LP600	medium	
K02017.01	12.888	2012/08/30	i	medium	
K02022.01	14.551	2012/09/13	LP600	medium	
K02025.01	13.608	2012/09/13	LP600	high	
K02026.01	13.121	2012/08/30	i	medium	
K02029.01	12.694	2012/09/13	LP600	high	
K02033.01	13.476	2012/08/30	i	medium	
K02035.01	12.782	2012/08/31	i	medium	
K02038.01	14.548	2012/10/06	LP600	medium	
K02040.01	13.983	2012/10/06	LP600	high	
K02042.01	12.941	2012/08/31	i	low	
K02044.01	15.591	2012/08/30	LP600	low	
K02045.01	15.135	2012/09/13	LP600	low	
K02046.01	12.939	2012/08/30	i	medium	
K02047.01	13.845	2012/10/06	LP600	high	
K02049.01	13.771	2012/10/06	LP600	high	
K02051.01	14.902	2012/09/13	LP600	low	
K02053.01	12.839	2012/09/13	LP600	high	
K02057.01	14.432	2012/07/16	LP600	medium	
K02058.01	14.78	2012/07/16	LP600	low	
K02059.01	12.558	2012/10/06	LP600	high	yes
K02071.01	13.478	2012/08/30	i	medium	
K02072.01	13.215	2012/08/30	i	medium	
K02073.01	15.225	2012/09/13	LP600	medium	
K02079.01	12.709	2012/08/30	i	medium	
K02082.01	13.964	2012/10/06	LP600	high	
K02086.01	13.776	2012/10/06	LP600	high	

TABLE 5 — *Continued*

KOI	$m_i$ / mags	Obs. date	Filter	Obs. qual.	Companion?
K02087.01	11.727	2012/08/30	i	high	
K02090.01	14.88	2012/07/16	LP600	low	
K02105.01	13.693	2012/10/06	LP600	high	
K02110.01	12.071	2012/08/30	i	high	
K02111.01	14.674	2012/09/13	LP600	low	
K02119.01	13.799	2012/10/06	LP600	high	
K02133.01	12.104	2012/08/31	i	medium	
K02135.01	13.416	2012/08/30	i	medium	
K02137.01	13.489	2012/08/30	i	medium	
K02138.01	12.127	2012/08/30	i	high	
K02143.01	13.872	2012/10/06	LP600	high	yes
K02149.01	11.928	2012/08/30	i	high	
K02158.01	12.796	2012/07/28	i	medium	
K02159.01	13.293	2012/08/31	i	medium	yes
K02162.01	13.864	2012/10/06	LP600	high	
K02169.01	12.172	2012/09/13	LP600	high	
K02173.01	12.522	2012/09/13	LP600	high	
K02175.01	12.626	2012/10/06	LP600	high	
K02191.01	14.275	2012/07/17	LP600	medium	
K02194.01	13.681	2012/08/31	i	low	
K02201.01	13.618	2012/10/06	LP600	high	
K02202.01	13.842	2012/08/31	i	low	
K02204.01	13.8	2012/10/06	LP600	medium	
K02215.01	12.699	2012/08/31	i	medium	
K02219.01	13.781	2012/08/31	i	low	
K02220.01	14.48	2012/09/13	LP600	low	
K02222.01	12.875	2012/08/31	i	medium	
K02224.01	14.742	2012/09/13	LP600	medium	
K02228.01	12.61	2012/10/06	LP600	high	
K02238.01	14.037	2012/07/17	LP600	medium	
K02246.01	13.965	2012/08/31	i	low	
K02252.01	13.471	2012/08/31	i	medium	
K02260.01	12.05	2012/08/31	i	high	
K02272.01	12.747	2012/08/31	i	high	
K02273.01	12.553	2012/08/31	i	medium	
K02276.01	11.485	2012/08/31	i	high	
K02279.01	13.688	2012/10/06	LP600	high	
K02281.01	13.535	2012/10/06	LP600	high	
K02287.01	12.1	2012/08/31	i	high	
K02289.01	13.193	2012/08/31	i	medium	
K02300.01	13.799	2012/08/31	i	low	
K02303.01	13.71	2012/10/06	LP600	high	
K02312.01	12.586	2012/08/31	i	high	
K02319.01	13.224	2012/08/31	i	medium	
K02331.01	13.29	2012/08/31	i	medium	
K02332.01	12.766	2012/08/31	i	medium	
K02335.01	13.912	2012/10/06	LP600	high	
K02342.01	12.87	2012/08/31	i	medium	
K02347.01	14.369	2012/07/17	LP600	low	
K02352.01		2012/09/14	LP600	high	
K02358.01	13.383	2012/08/31	i	medium	
K02365.01	13.682	2012/10/06	LP600	medium	
K02366.01	12.337	2012/08/31	i	high	
K02367.01	12.475	2012/10/06	LP600	high	
K02370.01	12.878	2012/07/28	i	medium	
K02374.01	14.371	2012/09/14	LP600	low	
K02389.01	13.417	2012/08/31	i	low	
K02390.01	12.08	2012/08/31	i	high	
K02398.01	13.437	2012/08/31	i	medium	
K02399.01	13.833	2012/10/06	LP600	medium	
K02407.01	13.979	2012/08/31	i	low	
K02408.01	13.972	2012/08/31	i	low	
K02410.01	14.949	2012/09/14	LP600	low	
K02413.01	14.684	2012/09/14	LP600	low	yes
K02414.01	13.39	2012/09/14	LP600	medium	
K02426.01	13.658	2012/10/06	LP600	high	
K02433.01	15.041	2012/09/14	LP600	low	
K02440.01	13.762	2012/10/06	LP600	high	
K02443.01	13.83	2012/10/06	LP600	high	yes
K02457.01	12.267	2012/08/31	i	medium	
K02463.01	12.609	2012/08/31	i	medium	yes
K02470.01	13.448	2012/08/31	i	medium	
K02479.01	12.687	2012/10/06	LP600	high	
K02481.01	13.214	2012/08/31	i	medium	

TABLE 5 — *Continued*

KOI	m <sub>i</sub> / mags	Obs. date	Filter	Obs. qual.	Companion?
K02484.01	12.293	2012/08/31	i	high	
K02486.01	12.89	2012/08/31	i	medium	yes
K02488.01	13.395	2012/08/31	i	medium	
K02498.01	13.678	2012/10/06	LP600	high	
K02503.01	13.781	2012/08/31	i	medium	
K02522.01	13.356	2012/08/31	i	medium	
K02527.01	13.67	2012/10/06	LP600	high	
K02530.01	13.436	2012/08/31	i	medium	
K02533.01	12.967	2012/08/31	i	medium	
K02534.01	13.755	2012/10/06	LP600	high	
K02538.01	13.847	2012/10/06	LP600	high	
K02541.01	12.717	2012/08/31	i	medium	
K02545.01	11.63	2012/08/31	i	high	
K02547.01	13.976	2012/10/06	LP600	high	
K02555.01	12.756	2012/10/06	LP600	high	
K02556.01	13.828	2012/10/06	LP600	medium	
K02559.01	13.626	2012/08/31	i	medium	
K02561.01	13.49	2012/08/31	i	medium	
K02563.01	13.82	2012/10/06	LP600	high	
K02564.01	13.91	2012/10/06	LP600	high	
K02581.01	13.248	2012/08/31	i	medium	
K02582.01	13.45	2012/08/31	i	medium	
K02583.01	12.423	2012/10/06	LP600	high	
K02585.01	13.311	2012/08/31	i	medium	
K02593.01		2012/08/31	i	high	
K02595.01	13.107	2012/08/31	i	medium	
K02597.01	14.626	2012/09/14	LP600	low	
K02603.01	12.457	2012/10/06	LP600	high	
K02608.01	13.124	2012/08/31	i	medium	
K02631.01	13.295	2012/08/31	i	medium	
K02632.01	11.28	2012/08/31	i	high	
K02640.01	12.896	2012/08/31	i	medium	
K02641.01	13.63	2012/10/06	LP600	high	yes
K02657.01	12.655	2012/10/06	LP600	high	yes
K02662.01	13.739	2012/07/17	LP600	medium	